4814–4830 *Nucleic Acids Research, 2023, Vol. 51, No. 10* *Published online 17 March 2023*
https://doi.org/10.1093/nar/gkad180

Spt6 directly interacts with Cdc73 and is required for Paf1 complex occupancy at active genes in *Saccharomyces cerevisiae*

Mitchell A. Ellison[1,†], Sanchirmaa Namjilsuren[1,†], Margaret K. Shirra[1], Matthew S. Blacksmith[1], Rachel A. Schusteff[1], Eleanor M. Kerr[1], Fei Fang[2], Yufei Xiang[2], Yi Shi[2] and Karen M. Arndt[1,*]

[1]Department of Biological Sciences, University of Pittsburgh, Pittsburgh, PA 15260, USA and [2]Department of Cell Biology, University of Pittsburgh, Pittsburgh, PA 15261, USA

Received April 29, 2022; Revised February 21, 2023; Editorial Decision February 23, 2023; Accepted February 28, 2023

ABSTRACT

The Paf1 complex (Paf1C) is a conserved transcription elongation factor that regulates transcription elongation efficiency, facilitates co-transcriptional histone modifications, and impacts molecular processes linked to RNA synthesis, such as polyA site selection. Coupling of the activities of Paf1C to transcription elongation requires its association with RNA polymerase II (Pol II). Mutational studies in yeast identified Paf1C subunits Cdc73 and Rtf1 as important mediators of Paf1C association with Pol II on active genes. While the interaction between Rtf1 and the general elongation factor Spt5 is relatively well-understood, the interactions involving Cdc73 have not been fully elucidated. Using a site-specific protein cross-linking strategy in yeast cells, we identified direct interactions between Cdc73 and two components of the Pol II elongation complex, the elongation factor Spt6 and the largest subunit of Pol II. Both of these interactions require the tandem SH2 domain of Spt6. We also show that Cdc73 and Spt6 can interact *in vitro* and that rapid depletion of Spt6 dissociates Paf1 from chromatin, altering patterns of Paf1C-dependent histone modifications genome-wide. These results reveal interactions between Cdc73 and the Pol II elongation complex and identify Spt6 as a key factor contributing to the occupancy of Paf1C at active genes in *Saccharomyces cerevisiae*.

INTRODUCTION

Eukaryotic cells deploy a large number of regulatory proteins to establish and maintain a chromatin template that both permits efficient transcription and prevents inappropriate or spurious transcription. Many of these proteins interact with Pol II during transcription elongation, when nucleosomes are dynamically modified, disrupted, and reassembled upon Pol II passage [reviewed in (1,2)]. Results from extensive genetic, biochemical, and structural studies in yeast and mammalian cells support a dynamic interplay in which transcription both regulates and is regulated by chromatin structure. Critical to this interplay are transcription elongation factors, histone chaperones, histone modifiers, and nucleosome remodeling enzymes.

The Polymerase Associated Factor 1 complex or Paf1C is a conserved member of the Pol II elongation complex found on actively transcribed regions of the genome (3–5). *Saccharomyces cerevisiae* Paf1C—consisting of the five subunits Paf1, Ctr9, Cdc73, Rtf1 and Leo1—was first discovered as a Pol II interacting complex engaged in functional and physical interactions with other transcription elongation factors (6–9). Subsequent studies showed that the complex is multifunctional [reviewed in (10)]. *In vitro* transcription reactions with purified factors showed that human Paf1C (hPaf1C) can stimulate transcription elongation on chromatin templates in cooperation with TFIIS (11). More recently, depletion of individual Paf1C subunits, including Paf1 and Rtf1, from human or mouse cell lines has revealed positive effects of the complex on elongation rate and Pol II processivity as well as context-dependent effects on promoter proximal Pol II pausing (12–17). The ability of hRtf1 to stimulate Pol II elongation rate *in vitro* involves an intimate contact

*To whom correspondence should be addressed. Tel: +1 412 624 6963; Email: arndt@pitt.edu
†The authors wish it to be known that, in their opinion, the first two authors should be regarded as Joint First Authors.
Present addresses:
Yufei Xiang, Center of Protein Engineering and Therapeutics, Department of Pharmacological Sciences, Icahn School of Medicine at Mount Sinai, New York, NY 10029, USA.
Yi Shi, Center of Protein Engineering and Therapeutics, Department of Pharmacological Sciences, Icahn School of Medicine at Mount Sinai, New York, NY 10029, USA.

between the hRtf1 latch domain and the Pol II catalytic center (5). Mutation or depletion of Paf1C also impairs processes coupled to transcription, including RNA 3′-end formation of noncoding RNAs, polyA site selection at protein-coding genes, mRNA export, and DNA damage repair (18–23).

In addition to directly affecting transcription elongation by Pol II, Paf1C regulates the epigenetic state of transcribed chromatin. In yeast, absence of Paf1, Ctr9, and to a lesser extent, Cdc73, leads to a decrease in H3 lysine 36 trimethylation (H3K36me3) (24). Enriched at the 3′ ends of genes, H3K36me3 promotes histone deacetylation by the Rpd3S complex, culminating in the restoration of a repressed chromatin state following Pol II passage [reviewed in (25)]. Another transcription-associated modification, H2B mono-ubiquitylation on K123 in *S. cerevisiae* (K120 in humans) is strongly dependent on a small conserved domain in Rtf1 (26–28) and is also stimulated by other subunits within the complex, including Ctr9 and Cdc73 (29). The Rtf1 histone modification domain (HMD) interacts directly with the ubiquitin conjugase Rad6 *in vivo* and can stimulate H2BK123ub in a reconstituted *in vitro* reaction (27). H2BK123ub initiates a cascade of downstream histone modifications with important roles in transcription, including di- and tri-methylation of H3 K4 and K79 [reviewed in (30)].

Coupling of the many functions of Paf1C to transcription elongation relies on its association with Pol II. Paf1C recruitment to the active Pol II elongation complex is dependent on the phosphorylation state of the Pol II C-terminal domain (CTD) of the Rpb1 subunit as well as the phosphorylation state of the Spt5 C-terminal repeat region (CTR) (31–35). The Spt5-Spt4 complex (DSIF in humans) is a highly conserved component of the active Pol II elongation complex along with Paf1C and Spt6, an essential histone chaperone and elongation stimulatory factor [reviewed in (36–38)]. A combination of genetic, biochemical and structural work has provided a molecular-level understanding of the Paf1C-Spt5 interaction. The central Plus3 domain of Rtf1 binds directly to the phosphorylated CTR of Spt5 (5,39–40). Mutation of the Rtf1 Plus3 domain, the Spt5 CTR, or the yeast CDK9 kinase Bur1, which phosphorylates the Spt5 CTR, greatly reduces Paf1C occupancy on coding regions (31–32,35,39–40). While the importance of the Spt5-Rtf1 interaction for Paf1C recruitment is well supported in yeast, it is unclear if a similar mechanism functions in mammalian cells where Rtf1 appears to be transiently associated with the other Paf1C subunits and may not provide a strong attachment point to Pol II (41).

In addition to a role for the Rtf1 Plus3 domain in coupling Paf1C to Pol II, we previously demonstrated that the C-terminal domain of yeast Cdc73, which has a Ras-like fold, is important for Paf1C localization to coding regions (42). However, significantly less is known about the interactions between Cdc73 and the Pol II elongation complex. While deletion of the Cdc73 C-terminal domain (hereafter, C-domain) reduced Paf1C occupancy on active genes, it did not affect Pol II occupancy or overall integrity of Paf1C. Biochemical insights into potential interacting partners for Cdc73 came from *in vitro* pulldown assays which detected interactions between Cdc73 and phosphorylated peptides derived from both the Pol II CTD and the Spt5 CTR (33). However, it is unclear if Cdc73 contacts Pol II or other members of the core elongation machinery *in vivo*.

In this study, we used site-specific crosslinking to identify interacting partners for Cdc73 *in vivo* and found that the Cdc73 C-domain directly interacts with two essential components of the Pol II elongation complex, Rpb1 and Spt6, in a manner that requires the tandem SH2 (tSH2) domain of Spt6. Discovery of the Cdc73-Spt6 interaction led us to investigate a broader role for Spt6 in regulating Paf1C occupancy on transcribed chromatin using acute Spt6 depletion. Our results show that Spt6 is critical for establishing and/or maintaining the occupancy of Paf1C and its chromatin-associated functions across the yeast genome.

MATERIALS AND METHODS

Yeast strains, growth conditions, and genetic manipulations

S. cerevisiae strains are isogenic to FY2, a *GAL2*$^{+}$ derivative of S288C (43) and are listed in Supplementary Table S1. Epitope tagging was achieved by one- or two-step integration into the yeast genome and confirmed by PCR (44). Yeast crosses and transformations were conducted as described (45). Strains containing the *rtf1-R251A, Y327A* allele integrated at the *RTF1* locus were created using *delitto perfetto* (46). A region of the *RTF1* gene (+710 to +990) was replaced with pCORE-UH (46) in strain KY3900 by homologous recombination, selecting for hygromycin^{R} Ura^{+} colonies to generate two independently derived integrants, KY3907 and KY3908. A DNA fragment of *RTF1* containing the R251A and Y327A substitutions was used to replace the pCORE region to generate KY3915 and KY3916. Finally, KY3917 and KY3918, strains for plasmid shuffling the *spt6* mutations, were made by transformation of KY3915 and KY3916 with pCK25, a *URA3*-marked plasmid containing *FLAG-SPT6* (47), followed by screening for Trp^{-} colonies that had lost pKB1623. *spt6* mutant strains were generated by plasmid shuffling with *TRP1*-marked *CEN/ARS* plasmids expressing N-terminal 3xV5-tagged WT Spt6 or mutant proteins (48). Transformants were passaged twice on synthetic complete medium (45) lacking tryptophan (SC-W) and containing 0.1% 5-fluoroorotic acid (5-FOA) to select against the *URA3*-marked *SPT6* plasmid. For auxin-induced degradation of Spt6, *SPT6-AID* cells, KY4305 and KY4306, were grown to log phase at 30°C in YPD medium (45) supplemented with 400 μM tryptophan (W). Indole-3-acetic acid (IAA; Sigma-Aldrich, I3750), dissolved in DMSO, was added to the culture at a final concentration of 500 μM before incubation at 30°C for the indicated time prior to crosslinking for chromatin immunoprecipitation (ChIP) or harvesting by centrifugation for western analysis and growth assays. For cell viability assays, IAA or DMSO treated *SPT6-AID* log-phase cultures were diluted 10-fold and mixed with methylene blue at a final concentration of 0.02% w/v. Cells were counted on a TC20 automated cell counter (BioRad).

Plasmid construction

Plasmid DNA was purified from *Escherichia coli* DH5α cells using a GeneJET Plasmid Miniprep kit (ThermoFisher

Scientific K0503). Plasmids were generated by standard restriction digests, site-directed mutagenesis, or Gibson assembly (New England Biolabs E2611S) and verified by DNA sequencing. In plasmid pCK858 (gift from Craig Kaplan), a modification of *RPB1* with a TEV protease cleavage site positioned after amino acid 1460 is inserted into vector pRS315 (49). Plasmids are listed in Supplementary Table S2 and sequences are available upon request.

Yeast extract preparation and western analysis

Protein extracts used in western analysis were prepared from log-phase cultures of yeast cells by TCA (50) or post-alkaline extraction (51) or by bead-beating in RIPA buffer, TEV cleavage buffer (50 mM Tris–HCl pH 8.0, 0.5 mM EDTA pH 8.0, 1 mM DTT, 1 mM PMSF) (27) or PreScission cleavage buffer (50 mM Tris–HCl pH 8.0, 50 mM NaCl, 1 mM EDTA pH 8.0, 0.1% NP-40, 1 mM DTT, 1 mM PMSF). Proteins were resolved on SDS-PAGE gels and transferred to nitrocellulose membranes. Blocking was carried out for 1–2 h at room temperature in TBST containing 5% milk. Antibodies that recognize the following proteins and epitope tags were used: glucose-6-phosphate dehydrogenase (G6PDH; Sigma-Aldrich A-9521, 1:20 000 or 1:50 000), H2B (Active motif 39237, 1:2000), H2BK123ub (Cell Signaling 5546, 1:1000), H3K4me2 (Millipore 07-030, 1:2000), H3K4me3 (Active Motif 39159, 1:2000), HA tag (Roche 11666606001, 1:1000 or 1:3000), His tag (Abcam ab18184, 1:1000), HSV tag (Sigma-Aldrich H6030, 1:1000 or 1:2000), Rpb1-Core (Y80 Santa Cruz, SC-25758, 1:1000), Rpb1-CTD (8WG16 BioLegend, 664906, 1:500), Rpb3 (BioLegend 665004, 1:1000), Rtf1 (1:5000 or 1:2500 dilution) (9), Spt5 (gift from Grant Hartzog, 1:1000), Spt6 (gift from Tim Formosa, 1:1000), and V5 tag (Invitrogen R960-25, 1:1000). Primary antibody incubations were carried out overnight at 4°C with agitation. Incubations with anti-mouse (Cytiva NA931) or anti-rabbit (Cytiva NA934) secondary antibodies (1:5000) were performed at room temperature for 1–2 h. Visualization of signals was achieved using Pico Plus chemiluminescence substrate (ThermoFisher Scientific 34580) and the ChemiDoc XRS imaging platform (BioRad). Quantifications were performed using Image Lab (BioRad).

In vivo photocrosslinking

BPA (p-benzoyl-L-phenylalanine) crosslinking experiments were performed as described (27,52). Briefly, yeast strains BTY42 (Figure 1), KY2838 (Figure 2B), KY4320 (Figure 2B), KY303 (Figure 2C) and KY3351 (Figure 2C) were co-transformed with pLH157/*LEU2* (Figures 1 and 2C) or pLH157/*TRP1* (Figure 2B), the tRNA/tRNA synthetase plasmids for BPA incorporation, and either a *TRP1*-marked (Figure 1) or *URA3*-marked plasmid (Figure 2) harboring *cdc73* with an amber codon substitution at the position of interest to allow for BPA incorporation by nonsense suppression (53). Yeast cells were grown to log phase in SC medium lacking the appropriate nutrients for plasmid selection and containing 1 mM BPA (Bachem F-2800). Crosslinking was performed as described (27). For Figures 1 and 2C, protein extracts were prepared by TCA extraction and analyzed by western blotting. For Figure 2B, 50 ml of cells in log phase were harvested for crosslinking. Following the UV exposure (365 nm), extracts were prepared from cell pellets by bead-beating in 500 μl of TEV or PreScission cleavage buffer and quantified by Bradford assay. For TEV cleavage experiments, one half of the extract was incubated at 25°C for 1.5 h with 4 μl of TEV protease (Invitrogen 12575-015). For PreScission cleavage experiments, 1.5 mg of protein extract in 160 μl of buffer was incubated overnight with 2.5 U PreScission protease (GenScript Z02799). Western blot analysis was performed on 75 μg of extract.

Recombinant protein expression and purification

Proteins were expressed in *E. coli* CodonPlus RIPL cells using the IPTG induction method. Expression plasmids are listed in Supplementary Table S2. Cells were grown at 37°C to an OD_{600} of 0.6–0.8 before the addition of 150 μM IPTG and incubation overnight at 25°C. Harvested cell pellets were lysed in Lysis Buffer [Buffer A (25 mM Tris–Cl pH 8.0, 10% glycerol, 1 mM beta-mercaptoethanol (βME)) with 500 mM NaCl and 25mM imidazole] by either homogenization or sonication in the presence of a protease inhibitor cocktail containing phenylmethylsulfonyl fluoride, aprotinin, leupeptin, and pepstatin. Lysates were centrifuged at 14000 rpm for 30 min at 4°C to isolate soluble protein. A combination of nickel affinity chromatography (Qiagen 30210) and cation exchange (GE Healthcare HiTrap-SP; Cdc73) or heparin affinity (GE Healthcare HiTrap-Heparin; Spt6) chromatography was used to purify 10xHis-mClover-Cdc73, Cdc73-10xHis, 10xHis-mClover-Spt6 and 10xHis-mRuby2-Spt6 fusion proteins. For nickel affinity chromatography, Lysis Buffer was used as the loading and wash buffer, and the elution buffer was Buffer A with 100 mM NaCl and 250 mM imidazole. For subsequent ion exchange and heparin affinity chromatography, the NaCl concentration was reduced to 50 mM by dilution with Buffer A prior to column loading, and fractions were taken in 100 mM NaCl steps starting at 100 mM and ending at 1 M. Fractions were collected by passing buffer through the column by hand using a lure lock syringe. Where indicated, the 10xHis tag and accompanying fluorescent protein (mClover or mRuby) were removed by TEV protease digest prior to heparin affinity or cation exchange chromatography. TEV digests were performed overnight, typically at 4°C, in dialysis tubing placed in a minimum of 2 l dialysis buffer (Buffer A with 100mM NaCl). Spt6-239-1451 used in chemical crosslinking and mass spectrometry experiments was further purified by size exclusion chromatography (GE Healthcare Sephacryl S-200) and anion exchange chromatography (GE Healthcare HiTrap-Q). Purified proteins were concentrated and exchanged into Binding Buffer (50 mM HEPES pH 8.0, 100 mM potassium acetate, 5 mM magnesium acetate, 10% glycerol and 1 mM βME). Buffer exchange was accomplished using Vivaspin concentrators (Sartorius). Protein purity was assessed by SDS-PAGE followed by Coomassie blue staining. A Nanodrop (ThermoFisher Scientific) was used to measure the concentrations of proteins that were not tagged with a fluorophore. Concentrations of fluorescently tagged proteins and any protein used for a quantitative binding assay were deter-

mined by SDS-PAGE, using a standard curve (lysozyme or bovine serum albumin) for quantitative comparison.

Native gel-shift assays

Binding reactions, performed in Binding Buffer (above), contained 150nM 10xHis-mClover-Cdc73 or 10xHis-mClover as a control and a range of concentrations of 10xHis-mRuby2-Spt6 (239–1451) or 10xHis-mRuby2-Spt6 truncation derivatives, as indicated. Reactions were incubated for 10 min at room temperature before loading on the gels. Agarose gels (0.5%) were cast and run using native agarose gel buffer (25 mM Tris–Cl pH 8.0, 19.2 mM glycine) at 120 V for 1.5 h at 4°C and imaged on an Amersham Imager 600. The gel and buffer were allowed to equilibrate to 4°C for at least 1 h before gels were loaded. Native gel-shift data were quantified by measuring the intensity of the 10xHis-mClover-Cdc73 band or the 10xHis-mClover control band. Band intensity values were measured from the raw TIFF files produced by the imager using LiCor ImagStudioLite. Fraction shifted was calculated using the following equation: fraction shifted = (shifted band intensity)/(shifted band intensity + unshifted band intensity). Curve fitting was performed with Prism 8 graphing software and the following equation: $Y = B_{max}*X/(K_d + X)$ + baseline. B_{max}, K_d and baseline were optimized for curve fitting.

Fluorescence anisotropy

100 nM 10xHis-mClover-Cdc73 was mixed with Spt6 (239–1451) in amounts ranging from 750 pM to 7.5 μM in Binding Buffer (see above) in black Nunc 384-Well Polystyrene microplates (ThermoFisher Scientific 262360) at a final reaction volume of 80 μl. Data were collected on a Cytation 5 plate reader (Agilent Technologies) using a green fluorescent polarization filter (excitation and emission wavelengths of 485 nm and 528 nm, respectively) and Gen5 software (BioTek). Curve fitting was performed with Prism 8 graphing software using the following equation: $Y = B_{max}*X/(K_d + X)$ + baseline. B_{max}, K_d and baseline were optimized for curve fitting and X was equal to mean change in anisotropy.

In vitro protein crosslinking experiments and mass spectrometry

Crosslinking experiments with DSS (disuccinimidyl suberate, ThermoFisher Scientific 21655) and EDC (1-ethyl-3-(3-dimethylaminopropyl)carbodiimide hydrochloride, ThermoFisher Scientific 22980) were conducted essentially as described with some modifications (54–56). Reactions were performed in a final volume of 20 μl. Proteins were added to either DSS crosslinking buffer/Binding Buffer (50 mM HEPES pH 8.0, 100 mM potassium acetate, 5 mM magnesium acetate, 10% glycerol, and 1 mM βME) or EDC crosslinking buffer (100 mM MES pH 6.0, 100 mM NaCl, 5 mM $MgCl_2$ and 10% glycerol) at a final concentration of 10 μM 10xHis-mClover-Cdc73 and 2 μM Spt6 (239–1451). DSS was dissolved in 100% DMSO and added at a final concentration of 625 μM (1 μl of 12.5 mM stock), and uncrosslinked controls were treated with 1 μl of 100% DMSO. For EDC crosslinking, EDC and NHS (N-hydroxysuccinimide, ThermoFisher Scientific 24500) were dissolved in water and added at a final concentration of 12.5 mM (EDC, 1 μl of 250 mM) and 250 μM (NHS, 1 μl of 5 mM), respectively, to achieve an EDC:NHS ratio of 50:1. Uncrosslinked control reactions for EDC samples were prepared by addition of 1 μl of water and 1 μl of 5 mM NHS. Reactions were incubated with agitation for 30 min at room temperature and then quenched by addition of 1 μl of 1M Tris–Cl pH 7.5 (DSS) or addition of both 1 μl of 1 M Tris–Cl pH 8.0 and 1 μl of 1 M BME (EDC), followed by agitation for 15 min at room temperature.

Products from DSS and EDC crosslinking reactions prepared for mass spectrometry analysis were combined with 7 μl of 3× SDS-PAGE loading dye lacking reducing agent, brought to a final concentration of 20 mM DTT by addition of 0.56 μl of 1 M DTT, and incubated at 75°C for 10 min. Samples were allowed to cool to room temperature for 5 min before addition of 1.43 μl iodoacetamide (Sigma A3221-10VL) dissolved in 80% distilled deionized water and 20% acetonitrile (ThermoFisher Scientific 85188) bringing the final concentration to 50 mM (2.5× that of DTT). Samples were incubated at room temperature for 30 min in the dark before running 20 μl of the reaction on an SDS-PAGE gel (4–12% Bis/Tris; NuPage NP0321). Crosslinked products were verified by western analysis. For mass spectrometry, bands containing crosslinked products were excised from the gel and destained. In-gel digestion of proteins with trypsin and Lys-C and subsequent steps in the LC/MS analysis were performed using a QE HFX Orbitrap mass spectrometer as previously described (55–58). No more than three missing trypsin cleavage sites were allowed. The raw MS data were searched using pLink2 (59). Search results obtained using a 5% false discovery rate were inspected manually to remove potential false positives as previously described (55–58).

Determining a structural model from crosslinking (XL)/MS data

The xiView web tool was used to generate a 2D network model of the crosslinking data, and structural modeling was performed using the Integrative Modelling Platform (IMP) (60). Prior to modeling with IMP, a prediction of full-length Cdc73 was generated via I-TASSER (61–63). The best prediction of full-length Cdc73 was determined by two metrics: 3D alignment to Cdc73 structures (3V46, 5YDE and 6AF0; (42,64–65)) and the number of valid crosslink lengths by XL-MS that satisfied a 30 Å cutoff. The crosslinking data used when choosing the best prediction were from a separate intramolecular XL-MS experiment on Cdc73-10xHis without Spt6 present (Supplementary Table S5). This model of *S. cerevisiae* Cdc73 was then used in IMP modeling. Spt6 structural information used with IMP was generated by combining information from 3PSF and 3PSI structures (66) after 3D alignment using the FATCAT server (67–70). This allowed the majority of Spt6 core residues to be included.

The generation of a three-dimensional model was accomplished by IMP using EDC ($n = 2$) and DSS ($n = 3$) datasets,

predicted *S. cerevisiae* Cdc73, and Spt6 structural information as input. Crosslinking distances (C_α – C_α) of 20 Å for EDC and 35 Å for DSS were used as constraints for IMP modelling (55). Only inter-protein crosslinks between Cdc73 and Spt6 core were considered in the modeling. During modeling, the position of the Spt6 core was held constant by specifying it as a fixed rigid body, and the Cdc73 structure was allowed to move in order to sample the various Cdc73-Spt6 interaction configurations. The top-scoring models were determined by running the IMP Monte-Carlo (MC) simulation over 100 000 frames with 10 MC steps per frame (1 000 000 steps total). To recover side-chain information, the structural information input into IMP was aligned back to the carbon alpha trace returned by IMP. This step was performed using the alignment plugin in PyMOL. Only Cdc73 data from the 3V46 structure of Cdc73, as defined by the top scoring model, was included in the final model (Figure S3F). Further information on the modeling of the Cdc73–Spt6 interaction, including PDB files, scripts, and crosslinking data, can be accessed on Zenodo (https://doi.org/10.5281/zenodo.7675568).

Chromatin immunoprecipitation (ChIP)

ChIP was performed essentially as described previously (71,72). Briefly, 200 or 250 ml of cell cultures were grown to log phase (OD_{600} = 0.8–1.0). Cells were crosslinked for 20 min at room temperature by addition of formaldehyde to 1% (v/v). Lysates were prepared in FA lysis buffer (73). Chromatin was sheared in Bioruptor® Pico 15 ml tubes with 300 µl beads (Diagenode C30010017) by 25 cycles of 30 s on and 30 s off using a Bioruptor® (Diagenode B01060010). Sonicated chromatin was brought up to a volume of 6 ml in FA lysis buffer and centrifuged at 50 000 rpm for 20 min at 4°C. Chromatin in the supernatant was aliquoted, flash-frozen, and stored at –80°C.

IP reactions were carried out after thawing chromatin on ice and bringing the NaCl concentration to 275 mM. For Figure 2 and Supplementary Figure S1, 350 µl IP reactions contained chromatin prepared as above and anti-Spt6 (gift from Tim Formosa, 2.5 µl), anti-Spt5 (gift from Grant Hartzog, 0.5 µl), anti-HSV (Sigma-Aldrich H6030, 1.25 µl), anti-Rtf1 (1 µl; (9)), anti-Rpb3 (BioLegend 665004, 1.25 µl) primary antibodies. For all other ChIP experiments, *S. cerevisiae* chromatin was mixed with *Schizosaccharomyces pombe* chromatin (KP08 for 8WG16 and HSV IPs or KP07 for all other IPs including those in Supplementary Figure S4) at a 9:1 (Supplementary Figure S4) or 10:1 ratio (*S. cerevisiae* : *S. pombe*) based on protein concentration (Pierce BCA protein assay kit; Thermo Fisher Scientific 23227), and IP reactions were conducted with anti-V5 (Invitrogen R960-25, 1 µl/225 µg or 10 µl/1800 µg), anti-Rpb1-CTD (8WG16; BioLegend 664906, 1 µl/225 µg or 8 µl/1800 µg), anti-HSV (Sigma-Aldrich H6030, 1.75 µl/450 µg or 7 µl/1800 µg), anti-HA (Santa Cruz sc-7392 AC, 15 µl/225 µg), anti-Spt5 (gift from Grant Hartzog, 4 µl/1800 µg), anti-H2BK123ub (Cell Signaling 5546, 5 µl/1000 µg), anti-total H3 (Abcam ab1791, 2 µl/1000 µg), anti-H3K4me2 (Millipore 07–030, 5 µl/1000 µg), anti-H3K4me3 (Active motif 39159, 5 µl/1000 µg), or anti-Myc (gift from John Woolford, used as a non-specific IgG control, 5 µl/1000 µg) primary antibodies. While *S. pombe* chromatin was included for the ChIP assays in Supplementary Figure S4, it was not used for normalization of the *S. cerevisiae* data as it increased variance in the qPCR measurements. IP reactions were incubated overnight at 4°C on an end-over-end roller. Protein A or G beads (Cytiva 17-5280-01 or 17-0618-01) were washed with FA lysis buffer with 275 mM NaCl and added to the chromatin-antibody mixture and placed on the roller for 1 hr at room temperature. Beads were washed and DNA recovered as previously described (72). DNA was purified using the QIAquick PCR Purification Kit (Qiagen, 28106).

ChIP quantitative polymerase chain reaction (ChIP-qPCR)

ChIP-qPCR experiments were performed using qPCRBIO SyGreen Blue 2× reaction mix (Genesee Scientific 17-505B) and analyzed on a QuantStudio3™ Real-Time PCR System (Thermo Fisher). Efficiencies were determined for primer sets by measuring C_t values across a series of six 10-fold dilutions of *S. cerevisiae* genomic DNA. ChIP-qPCR data were analyzed as described previously (74) and normalized as indicated in the figure legends. Primer sequences and efficiencies are listed in Supplementary Table S3.

Next-generation sequencing library preparation

ChIP-sequencing (ChIP-seq) libraries were prepared using an NEBNext Ultra II kit and indices (E7645, E7335, E7500, E7710, E7730). AMPure XP beads (Beckman Coulter A63880) were used for DNA library clean-up. DNA libraries were quantified using a Qubit 4 fluorometer and fragment length distributions were assessed using a Fragment Analyzer (Advanced Analytical Technologies) with a Small Fragment Kit (Agilent DNF-476). DNA sequencing was conducted by the University of Pittsburgh Health Sciences Sequencing Core at UPMC Children's Hospital of Pittsburgh on an Illumina NextSeq 2000.

ChIP-seq data analysis

ChIP-seq reads were aligned to the *S. pombe* genome (Ensembl EF2) and then unaligned reads were aligned to the *S. cerevisiae* genome (Ensembl R64-1-1), using Bowtie2 (75) before SAM to BAM conversion, and PCR duplicate removal with the SAMtools suite (76). Spike-in normalization factors were calculated via a custom bash script using established methods (77). BAM to BigWig conversion was conducted while simultaneously applying the normalization factors. This was done by multiplying each base pair of the genome by the normalization factor using deepTools3 bamCoverage.

Biological replicate BigWig files were averaged using the bigwigCompare command and $\log_2$ fold change BigWigs were generated from these using the bigwigCompare command. Heatmaps and aggregation plots were plotted over genic regions using a bin size of 25 bp and averaging data within each bin using deepTools3 and a combination of the computeMatrix and either the plotHeatmap or plotProfile commands (78,79). Differential occupancy analysis was conducted in RStudio. ChIP-seq reads were counted from

BAM files for all protein-coding genes in the *S. cerevisiae* genome using the featureCounts function in the Rsubread package and used to generate count tables for DESeq2. Count tables were filtered prior to statistical analysis with DESeq2 to only include genes where the sum of the read counts across samples to be analyzed was greater than or equal to 10 reads. The spike-in normalization factors were applied to datasets during DESeq2 normalization. The DESeq2 and psych R packages were used to generate statistics on differential ChIP-seq occupancy presented in MA and correlation plots, respectively. Genome browser tracks were generated using IGV (80). Bash and R code as well as gene annotation files used for analysis are stored on Zenodo (https://doi.org/10.5281/zenodo.7675568).

Statistical analysis and reproducibility

BPA crosslinking experiments were performed at least twice using independent transformants. ChIP-qPCR experiments were performed in biological duplicate or triplicate and technical duplicate, unless noted otherwise. A minimum of three biological replicates were analyzed for the AID western blot and viability assay experiments. Each biological replicate is a pure yeast culture derived from a single colony. For ChIP analysis of *spt6 rtf1* double mutants in Supplementary Figure S4, two independent biological replicates were created from KY3917 and one from KY3918 through plasmid shuffling. Protein binding assays were performed at least four times. DSS and EDC crosslinking and mass spectrometry were performed in triplicate and duplicate, respectively, generating a total of five crosslinking datasets for model generation. Bar graphs plot mean and standard deviation and include all individual data points. For ChIP-qPCR data, *P*-values were generated using an unpaired, two-sided Student's *t*-test, assuming equal variance carried out between the mutant strain and the wild-type strain. Pearson's correlation analysis was used to assess replicate reproducibility and correlation between ChIP-seq datasets. Spearman's correlation analysis was used to compare $\log_2$ fold change datasets. Differential gene occupancy was determined using a negative binomial generalized linear model, which was implemented in R via the DESeq2 package.

RESULTS

Cdc73 directly interacts with Rpb1 and Spt6 *in vivo*

To identify interaction partners for Cdc73 *in vivo*, we employed a site-specific protein crosslinking strategy. Guided by our structural analysis of Cdc73 (42), we replaced surface-exposed amino acids on the Cdc73 C-domain (Figure 1A and B) with the photoreactive phenylalanine analog, BPA, through amber codon suppression (53). Based on the levels of full-length Cdc73 protein produced in cells grown in BPA-containing medium, BPA was incorporated at positions 268, 272, 300 and 321 while incorporation at position 319 was unsuccessful (Figure 1C). BPA-dependent, crosslinked products were produced upon exposure of cells to UV light at 365 nm, and these were detected by western blotting using an antibody against the HSV tag on Cdc73 (Figure 1C, lanes 6, 9, 12 and 18). Further resolution of

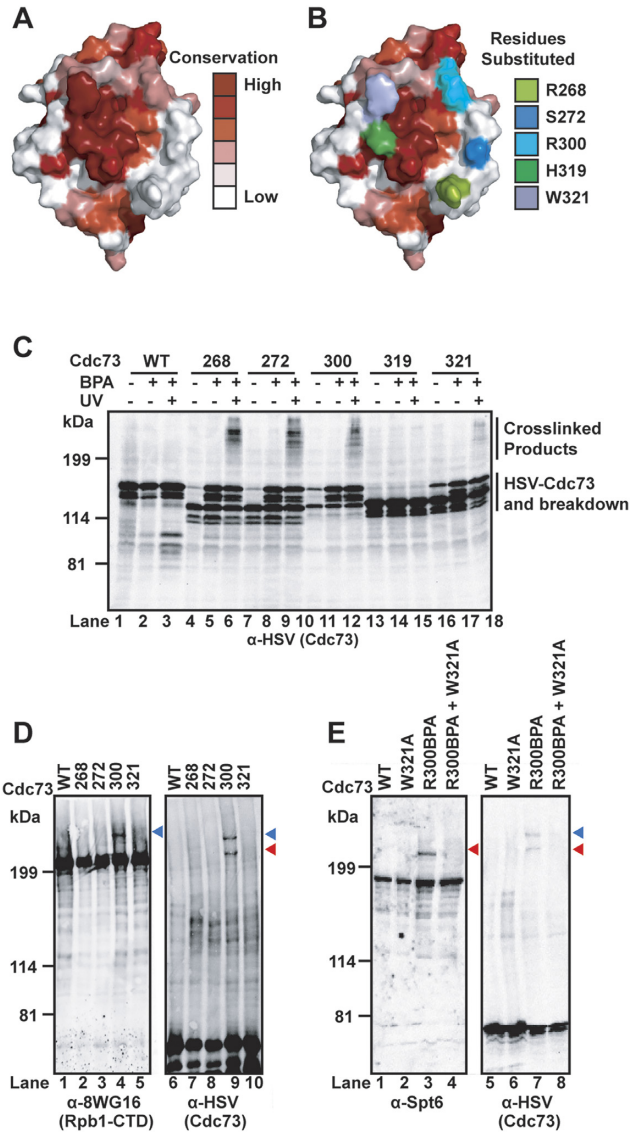

Figure 1. Detection of Cdc73 binding to Spt6 and Rpb1 *in vivo* by BPA crosslinking. (**A**) Cdc73 C-domain crystal structure (3V46) with conservation mapped using the Consurf server. (**B**) As in panel A except showing the locations of residues substituted with BPA. (C–E) Western analysis of protein extracts from BPA crosslinking experiments with the indicated antibodies. (**C**) Assessment of optimal location for BPA incorporation in N-terminally, triple HSV-tagged Cdc73. Cells were grown in the presence of BPA and exposed to UV radiation as indicated. Numbers above the lanes indicate the position of BPA incorporation in Cdc73. On the right, bands corresponding to crosslinked products and full-length HSV-Cdc73 are indicated. Bands below the full-length HSV-Cdc73 band correspond to truncated HSV-Cdc73 proteins that terminate at the amber codon and likely breakdown products. Note, depending on the mutant, we occasionally detect full-length protein in the absence of BPA, indicating endogenous translational readthrough of the amber codon (e.g. lane 16). (**D**) Cdc73-Rpb1 interaction (blue arrow) captured by BPA crosslinking. Adjacent panels were derived from the same gel. (**E**) Cdc73-Spt6 interaction (red arrow) captured by BPA crosslinking. Adjacent panels were derived from the same gel. In both panels D and E, the blue arrow marks the Cdc73-Rpb1 crosslinked product and the red arrow marks the Cdc73-Spt6 crosslinked product. All extracts analyzed in D and E were derived from cells grown in the presence of BPA and exposed to UV radiation. WT = wildtype.

the crosslinked species revealed two slowly migrating, HSV-reactive bands in the R300BPA sample. Western analysis identified the top band as a crosslinked product between HSV-Cdc73 and the largest Pol II subunit, Rpb1 (Figure 1D, lanes 4 and 9; blue arrow), and the bottom band as HSV-Cdc73 crosslinked to Spt6 (Figure 1E, lanes 3 and 7; red arrow).

To investigate the functional significance of the Cdc73-Rpb1 and Cdc73-Spt6 interactions, we performed BPA crosslinking experiments with an HSV-Cdc73 R300BPA derivative in which the highly conserved, surface-exposed tryptophan at position 321 was changed to alanine. We previously showed that the Cdc73 W321A substitution causes phenotypes associated with defects in transcription elongation (42). Crosslinking of both Rpb1 and Spt6 to HSV-Cdc73 R300BPA was greatly diminished by the W321A substitution suggesting that these interactions are dependent on a transcriptionally important residue within Cdc73 (Figure 1E).

Cdc73 R300BPA crosslinks to the Rpb1 linker *in vivo*

In previous studies, recombinant full-length Cdc73 and a C-domain containing fragment of Cdc73 exhibited binding to diphosphorylated Pol II CTD peptides *in vitro* (33). Our crosslinking data demonstrate that Cdc73 interacts directly with Rpb1 in cells. To further characterize this interaction and begin to map the site of interaction on Rpb1, we performed BPA crosslinking experiments on yeast cells expressing HSV-Cdc73 R300BPA and derivatives of Rpb1 engineered to contain either a TEV or PreScission protease cleavage site (Figure 2A) (81). Inserted after residue 1460, the TEV cleavage site is close to the Rpb1 core domain and separates the core from the Rpb1 linker region and CTD (82). Following TEV protease treatment of extracts prepared from UV-exposed cells, the Cdc73-Rpb1 crosslinked product (Figure 2B, lane 5; blue line) shifted to a position on the gel (Figure 2B, lane 6; black line) that was inconsistent with crosslinking to the Rpb1 core domain (Figure 2B, lanes 14, 16, and 18; orange line denotes the position of uncrosslinked Rpb1 core domain). Moreover, the TEV protease-cleaved Cdc73-Rpb1 product (Figure 2B, lane 6; black line) was detected with 8WG16 antibody, which recognizes the Pol II CTD (Figure 2B, lane 7; black line). Detection of the HSV- and 8WG16-reactive band (Figure 2B, lanes 6 and 7; black line) was dependent on the presence of BPA and UV treatment. These data map the site of Cdc73 R300BPA to a fragment of Rpb1 containing both the linker and CTD.

To further localize the site of Cdc73 R300BPA crosslinking on Rpb1, we used an Rpb1 derivative containing a PreScission protease site positioned after residue 1512 (81) (Figure 2A). Although the digest was incomplete, PreScission protease treatment of extracts from UV-exposed Cdc73 R300BPA cells generated a high molecular weight cleavage product that was detected by the HSV tag on Cdc73 and runs close to the Cdc73-Spt6 crosslinked species in western blots (Figure 2B, lanes 23 and 24; grey line). This crosslinked cleavage product was significantly larger than that generated with the Rpb1 construct containing the TEV protease site after residue 1460 (Figure 2B, lanes 24 and 26; compare grey and black lines). These data show that Cdc73 crosslinks to the large PreScission cleavage fragment, which contains the Rpb1 linker and core domains. Taken together, the protease mapping experiments localize the site of Cdc73 R300BPA crosslinking to the Pol II linker. While we cannot rule out other sites of contact between Cdc73 and Rpb1, our crosslinking results with the Cdc73 R300BPA derivative provide the first demonstration that Cdc73 directly contacts the Pol II linker and Spt6 *in vivo*.

The Spt6 tSH2 domain is required for crosslinking of Cdc73 R300BPA to Spt6 and Rpb1 and for Paf1C occupancy on active genes

Previous structural and genomic studies showed that the Rpb1 linker interacts with the tSH2 domain of Spt6 and is important for coupling Spt6 to Pol II on gene bodies (3,82). Moreover, in a very recent cryo-EM analysis of a Pol II elongation complex, the Cdc73 C-domain was found to interact with the Spt6 tSH2 domain (83). Prompted by these observations, we tested the importance of the Spt6 tSH2 domain for the Cdc73 interactions we detect *in vivo*. To this end, we performed BPA crosslinking experiments with a yeast strain containing the *spt6-50* mutation, a nonsense mutation that truncates the Spt6 tSH2 domain (66,82,84–87) (Supplementary Figure S1A and B). Strikingly, in the context of the *spt6-50* mutation, crosslinking of Cdc73 R300BPA to both Rpb1 and Spt6 was no longer detected (Figure 2C). To test if the loss of Cdc73 crosslinking to Rpb1 and Spt6 correlates with a loss of Paf1C on active genes, we performed ChIP-qPCR analysis of two highly transcribed genes, *PMA1* and *PYK1*, in *SPT6* and *spt6-50* strains (Figure 2D and Supplementary Figure S1C). Absence of the tSH2 domain reduced Spt6 occupancy on both genes, as expected, without significantly affecting Pol II or Spt5 occupancy (Figure 2D and Supplementary Figure S1C). Interestingly, although a slight reduction in total protein levels in the *spt6-50* mutant might contribute to the magnitude of the effect (Supplementary Figure S1B), we observed a strong reduction in the chromatin occupancy of HSV-Paf1 and Rtf1 in the *spt6-50* mutant. Collectively, our results are consistent with the idea that the Spt6 tSH2 domain is important for bridging interactions between Pol II, Spt6 and Paf1C and support a role for Spt6 in recruiting or retaining Paf1C on transcribing Pol II.

Cdc73 and Spt6 can interact directly *in vitro*

Because an interaction between Cdc73 and Spt6 had not been extensively characterized, we focused on this interaction and a possible role for Spt6 in controlling Paf1C occupancy at transcribed genes. To test if the Cdc73-Spt6 interaction can occur in the absence of other factors, we conducted *in vitro* binding assays with purified, recombinant Spt6 (239–1451) and full-length Cdc73 fused to 10xHis-mRuby2 and 10xHis-mClover tags, respectively (Figure 3A and Supplementary Figure S2A). The Spt6 (239–1451) derivative lacks an acidic, unstructured N-terminal region and has been used previously for structural studies (66). Native gel-shift assays, followed by detection and quantification of fluorescence signals, showed that the tagged

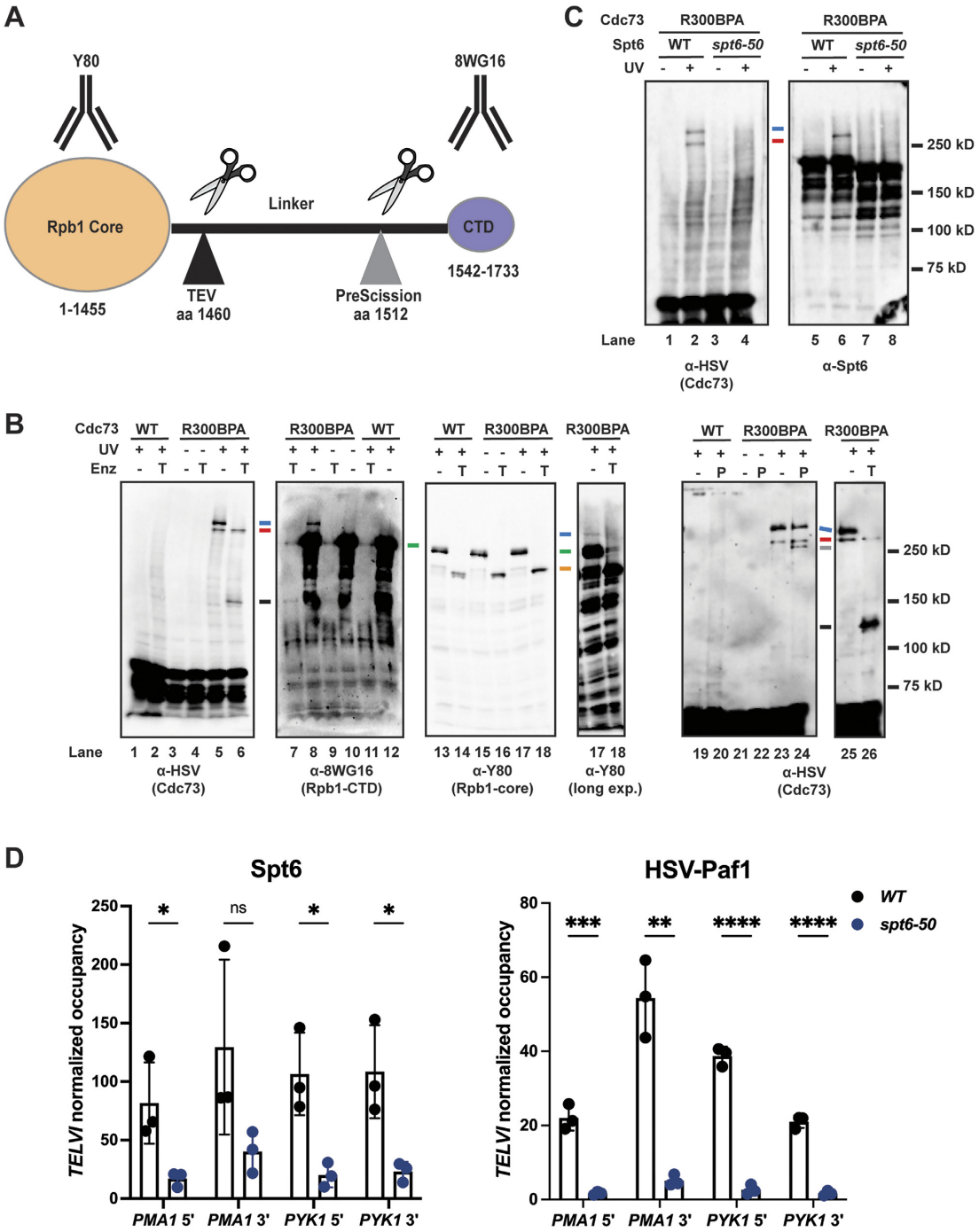

Figure 2. Crosslinking between Cdc73 and Rpb1 maps to the Rpb1 linker region and requires the Spt6 tSH2 domain. (**A**) Diagram depicting the locations of the TEV and PreScission protease cleavage sites in two different Rpb1 constructs used to map the site of Cdc73 R300BPA crosslinking in Rpb1. The Rpb1 construct containing the PreScission site also contains an 8XHis tag after the PreScission site and a C-terminal 3XFLAG tag (not shown). (**B**) TEV (T) or PreScission (P) protease cleavage of Rpb1 following UV-induced crosslinking to Cdc73 R300BPA. Lanes 1–18 are from the same gel. Lanes 19–26 are from the same gel. The red lines mark the position of the Spt6-Cdc73 crosslinked product, the blue lines mark the full-length Rpb1-Cdc73 crosslinked product prior to cleavage, the green lines mark the position of full-length, uncrosslinked Rpb1, the orange line marks the position of cleaved, uncrosslinked Rpb1 core domain, the black line marks the position of the Rpb1-Cdc73 product after TEV cleavage and the grey line marks the position of the Rpb1-Cdc73 product after PreScission cleavage. A longer exposure of lanes 17 and 18 is shown to reveal the Rpb1-Cdc73 crosslinked product (blue line) upon probing with the α-Y80 Rpb1 core domain antibody. Due to the presence of 8XHis and 3XFLAG tags, the Rpb1 protein containing the PreScission site is larger than that containing the TEV site, as indicated by the tilted blue line between lanes 24 and 25. (**C**) C-terminal truncation of Spt6, encoded by the *spt6-50* nonsense mutation, disrupts crosslinking of Cdc73 to both Spt6 and Rpb1. Bands are labeled as in panel B. (**D**) ChIP-qPCR analysis of Spt6 and HSV-Paf1 occupancy at the 5′ and 3′ ends of two highly expressed genes, *PMA1* and *PYK1*, in WT and *spt6-50* strains (KY3343 and KY3352). Data for target genes were normalized to input and to ChIP signals for a region near telomere VI. The mean and standard deviation of three biological replicates are plotted. Unpaired student's t test: ns, not significant; *$P < 0.05$; **$P < 0.01$; ***$P < 0.001$; ****$P < 0.0001$.

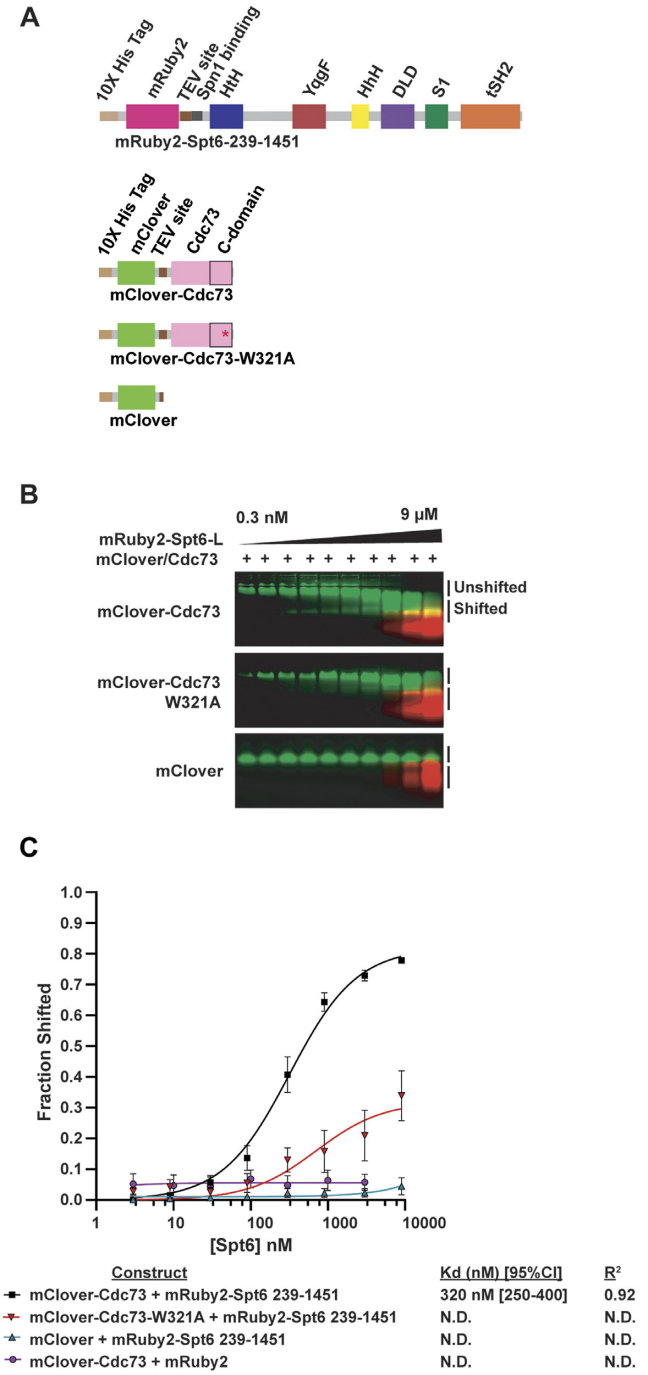

Figure 3. Cdc73 can bind directly to Spt6 *in vitro*. (**A**) Diagram of recombinant, fluorescently tagged proteins used for *in vitro* binding assays. Spt6 protein domain names and locations are as described by Close *et al.* (66). (**B**) Representative native gel-shift assays using recombinantly expressed fusion proteins as diagrammed in panel A and shown in Supplementary Figure S2A. mRuby2-Spt6-L (long) denotes the mRuby2-Spt6-239-1451 construct. (**C**) Quantified data from the gel-shift experiments shown in panel B and an mRuby2 control (representative shown in Figure S2D) plus a minimum of three additional replicates. Data were quantified by calculating the fraction of mClover-Cdc73 (green band) shifted. Binding curves and Kd values were determined in Prism as described in the Methods. N.D. = not determined

Spt6 (239–1451) and Cdc73 proteins can interact *in vitro* with a K_d of approximately 320 nM (Figure 3B and C). The W321A substitution in Cdc73 weakened this interaction (Figure 3B and C). Fluorescence anisotropy data collected using wild-type 10xHis-mClover-Cdc73 and unlabeled Spt6 (239–1451) support the gel-shift results but reported a lower binding affinity (K_d = 770 nM, Supplementary Figure S2B). Upon testing C-terminally truncated derivatives of 10xHis-mRuby2-Spt6 (Supplementary Figure S2A and C) (66), we found that removal of the tSH2 domain together with the S1 domain greatly reduced the interaction with 10xHis-mClover-tagged Cdc73 (Supplementary Figure S2D–E). An Spt6 truncation mutant lacking all structural domains C-terminal to the helix-turn-helix domain (HtH) was severely defective for Cdc73 binding (Supplementary Figure S2D–E), suggesting that the Spt6 core, which extends from the HtH domain through the S1 domain (66), is important for the interaction between purified Cdc73 and Spt6 *in vitro*.

To elucidate the interface between recombinant 10xHis-mClover-Cdc73 and untagged Spt6 (239–1451), we performed chemical crosslinking followed by mass spectrometry (see Methods) using two different crosslinking agents: DSS, which crosslinks lysine residues, and EDC, which crosslinks lysines to either glutamic acid or aspartic acid residues (55). Interprotein crosslinks were observed between Cdc73 and several conserved domains within the Spt6 core (Supplementary Figure S3A, Supplementary Table S4). With respect to Cdc73, most of the crosslinks mapped to the C-domain (between residues 263 and 371) and the region N-terminal to the C-domain (between residues 185 and 205). We used interprotein crosslinks from replicate experiments, Spt6 structural information, and a predicted model of full-length Cdc73 (see Methods and Tables S4 and S5) as input for the Integrative Modeling Platform (IMP) (60). The top 4 structural models produced by IMP aligned with an RMSD < 2.5 Å (Supplementary Figure S3B). The top-scoring model showed Cdc73 interacting with the Spt6 core in a depressed region between the death-like domain (DLD), the helix-hairpin-helix domain (HhH), and the YqgF domain (Supplementary Figure S3C–F and Supplementary Table S4). Residues W321 and R300 of Cdc73 face in toward the Spt6 core in this model (Supplementary Figure S3E–F).

Guided by our structural model, we generated alanine scanning substitutions in Spt6 that map within the predicted Cdc73-Spt6 interface and tested their effects on chromatin occupancy of Paf1C (Supplementary Figure S4A and B). By plasmid shuffling, plasmids harboring the *spt6* mutations were introduced into an *spt6Δ* strain or into an *spt6Δ rtf1-R251A, Y327A* strain. The latter contains substitutions at the interface between the Rtf1 Plus3 domain and the Spt5 CTR (40) and was used to test if the putative Cdc73-Spt6 interface functions redundantly with the Rtf1-Spt5 interaction in recruiting Paf1C to chromatin. Western analysis demonstrated that the V5-tagged Spt6 mutant proteins were expressed at near wild-type levels and did not affect the levels of Rpb1 or three different subunits of Paf1C, Paf1, Cdc73 and Rtf1 (Supplementary Figure S4C). ChIP-qPCR analysis showed that none of the individual alanine scanning substitutions significantly impacted Spt6

or Paf1C occupancy at the *PMA1* gene, although slight effects on Rpb1 occupancy were observed (Supplementary Figure S4D). While the *rtf1-R251A, Y327A* mutation decreased both Paf1 and Cdc73 occupancy at *PMA1* as expected (40), addition of the *spt6* mutations did not exacerbate this effect (Supplementary Figure S4D). Consistent with at least partial retention of Paf1C, H2BK123ub levels were unaffected by the *spt6* and *rtf1* mutations (Supplementary Figure S4C). These observations suggest that the proposed Cdc73-Spt6 interface is either not playing a major role in Paf1C recruitment or the individual *spt6* alanine-scanning mutations are insufficient to disrupt the Cdc73-Spt6 interaction.

Acute depletion of Spt6 leads to genome-wide loss of Paf1 occupancy and changes in histone modification patterns

Given our discovery of physical interactions between the Cdc73 C-domain and Spt6 as well as the reduction in chromatin occupancy of Paf1 in the *spt6-50* background, we investigated a role for Spt6 in globally controlling Paf1C occupancy at transcribed genes. To this end, we acutely depleted Spt6 through an auxin-inducible degron tag (88) appended to the C-terminus of Spt6, followed by ChIP-seq analysis of HSV-tagged Paf1 (Figure 4A). This approach allowed us to assess the effects of rapidly depleting Spt6 while minimizing cellular adaption to its loss and indirect effects. A viability assay confirmed that treatment of the *SPT6-AID* strain with auxin for two hours did not result in significant cell death relative to a DMSO-treated control sample (Supplementary Figure S5A). Western analysis demonstrated a reduction in Spt6 levels over a two-hour time course of auxin treatment with no adverse effect on HSV-Paf1 levels (Figure 4B and Supplementary Figure S5B).

As measured by spike-in normalized ChIP-seq analysis of two biological replicates, *SPT6-AID* cells treated with auxin for one hour showed a dramatic and statistically significant decrease in both Spt6 and HSV-Paf1 occupancy on chromatin compared to *SPT6-AID* cells treated with DMSO (Figure 4C–H; see Supplementary Figure S6 for correlations between samples and between replicates). In contrast to the effects on HSV-Paf1, rapid depletion of Spt6 caused a slight increase in both Rpb1 (8WG16) and Spt5 occupancy over gene bodies (Figure 4C–E, Supplementary Figure S5E–F), potentially due to increased internal transcription initiation events and/or reduced elongation rate in the absence of Spt6 (89–91). Correlation analysis of changes in occupancy profiles upon Spt6 depletion separated Spt5 and Rpb1 into one group and Paf1 and Spt6 into another (Figure 4F). In support of the ChIP-seq data, ChIP-qPCR measurements at specific highly and lowly expressed genes revealed a significant decrease in Spt6 occupancy at both gene classes and a significant decrease in Paf1 occupancy at two highly expressed genes (Supplementary Figure S5C and D). As measured by ChIP-qPCR, the occupancies of Rpb1 and Spt5 were not significantly affected at these genes (Supplementary Figure S5C and D). These data implicate Spt6 as a critical factor in controlling proper genome-wide localization of Paf1C in yeast.

Given the importance of Paf1C in promoting transcription-coupled histone modifications, we assessed the effects of rapidly depleting Spt6 on the genic patterns of H2BK123ub, H3K4me2 and H3K4me3 (see Supplementary Figure S7 for correlations between samples and between replicates). In agreement with previous studies on *spt6* mutant strains (77,92–93), a global reduction in H3 occupancy was observed when *SPT6-AID* cells were treated with auxin for one hour (Figure 5A–D). In addition to the general reduction in H3 occupancy, we observed a dramatic loss of H2BK123ub across gene bodies and a redistribution of H3K4me2 and H3K4me3 toward the 3′ ends of genes (Figure 5A–D). The reduction in H2BK123ub correlates with the loss of Paf1 occupancy observed upon Spt6 depletion (Figure 4; Supplementary Figure S8). The changes in H3K4me2 and H3K4me3 patterns upon Spt6 depletion correlate with one another (Supplementary Figure S8) and strongly agree with the results of Jeronimo *et al*. (77), who observed a 3′-directed redistribution of these marks in *spt6-1004* mutant cells or upon anchor-away depletion of Spt6. Redistribution of H3K4me3 was also observed upon acute depletion of Spn1, a histone chaperone that interacts with Spt6 (94). By demonstrating a requirement for Spt6 in the recruitment and/or retention of Paf1C on gene bodies, our results provide an additional mechanism through which Spt6 determines histone modification patterns genome-wide.

DISCUSSION

In this study, we investigated the coupling of Paf1C to the active Pol II elongation complex, focusing on the role of the Cdc73 subunit. Early studies in yeast revealed that null mutations in *CDC73* and *RTF1* dissociated Paf1C from chromatin and pointed to these two subunits as important mediators of the interaction of Paf1C with Pol II (95). The interaction between Rtf1, through its Plus3 domain, and the phosphorylated Spt5 CTR is understood at the structural level, and mutations that alter this interaction reduce Paf1C occupancy on chromatin in yeast (32,39–40). However, the interactions between Cdc73 and the Pol II elongation complex have not been fully defined, and until recently, structural information on Cdc73 within the elongation complex has been limited (4–5,83). We previously showed that the Cdc73 C-domain, which adopts a Ras-like fold, is required for full Paf1C occupancy on transcribed genes but not Paf1C assembly (42). Here we identify Spt6 and Rpb1 as direct interactors of Cdc73 *in vivo* and demonstrate a requirement for Spt6 in recruiting Paf1C to chromatin genome-wide.

Prior to this work, evidence suggested an important role for the phosphorylated Pol II CTD in recruiting Paf1C to chromatin. In both yeast and mammalian cells, inactivation of protein kinases that phosphorylate the CTD lower Paf1C occupancy on active genes or association of Paf1C with isolated elongation complexes (31,33–34,96). These kinases include Kin28/CDK8, which phosphorylates serines 5 and 7 of the CTD heptapeptide repeat, and Bur1/CDK9 and CDK12, which phosphorylate serine 2 of the repeat [reviewed in (97)]. Peptide pulldown assays with purified yeast Paf1C or isolated subunits provided more direct evidence for an interaction between Paf1C and the phosphorylated Pol II CTD. These studies detected binding of three

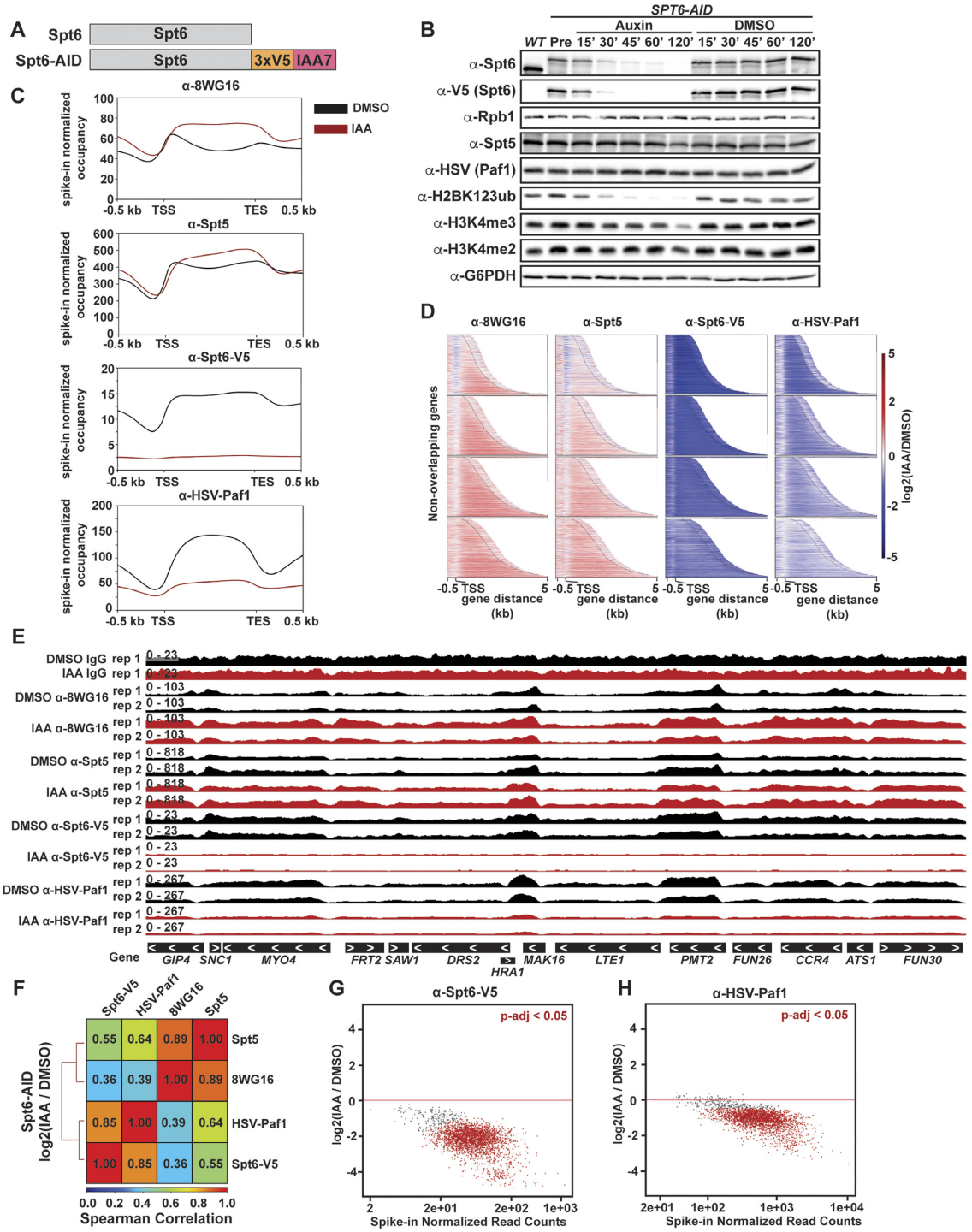

Figure 4. Acute depletion of Spt6 leads to nearly complete loss of Paf1 occupancy genome-wide. (**A**) Diagram comparing the proteins encoded by the *SPT6* and *SPT6-AID* genes. (**B**) Western analysis of *SPT6-AID* cells treated with IAA or DMSO for 0 (Pre), 15, 30, 45, 60 or 120 min. An untagged *SPT6* strain (WT), KY4343, was used as a control to measure the effect of the AID tag on Spt6 protein abundance. G6PDH serves as a loading control. Representative gels from three biological replicates are shown. (**C**) Aggregation plots of Rpb1 (8WG16), Spt5, Spt6-V5, and HSV-Paf1 spike-in normalized ChIP-seq occupancy. (**D**) Heatmaps of differential Rpb1, Spt5, Spt6-V5 and HSV-Paf1 occupancy (IAA vs DMSO). Genes are divided into quartiles based on Rpb1 occupancy (highest quartile is shown on the top) and sorted by length. Heatmaps show the region between the transcription start site (TSS) and the cleavage and poly-adenylation site (labeled with a black line) +/- 500 bp and use a bin size of 25 bp. (**E**) Genome browser tracks of a region of chromosome 1 (chrI:84656–118640) showing spike-in normalized ChIP-seq occupancy for individual biological replicates. An irrelevant antibody (anti-Myc) was used as the IgG background control for ChIP-seq (note the scale). To conserve space, one of two replicates of this control is shown (see Figure S6B for a comparison of replicates). (**F**) Heatmap of Spearman correlation between datasets plotted in D. (**G, H**) MA plots showing DESeq2 differential occupancy results for Spt6-V5 and HSV-Paf1 spike-in normalized ChIP-seq occupancy (IAA vs DMSO). Genes with statistically significant changes in occupancy (FDR-adjusted *P* value ≤ 0.05) are colored red. The results presented in panels C, D, F, G and H were generated by averaging spike-in normalized ChIP-seq data from two biological replicates (strains KY4305 and KY4306) for 3087 non-overlapping protein-coding genes (94).

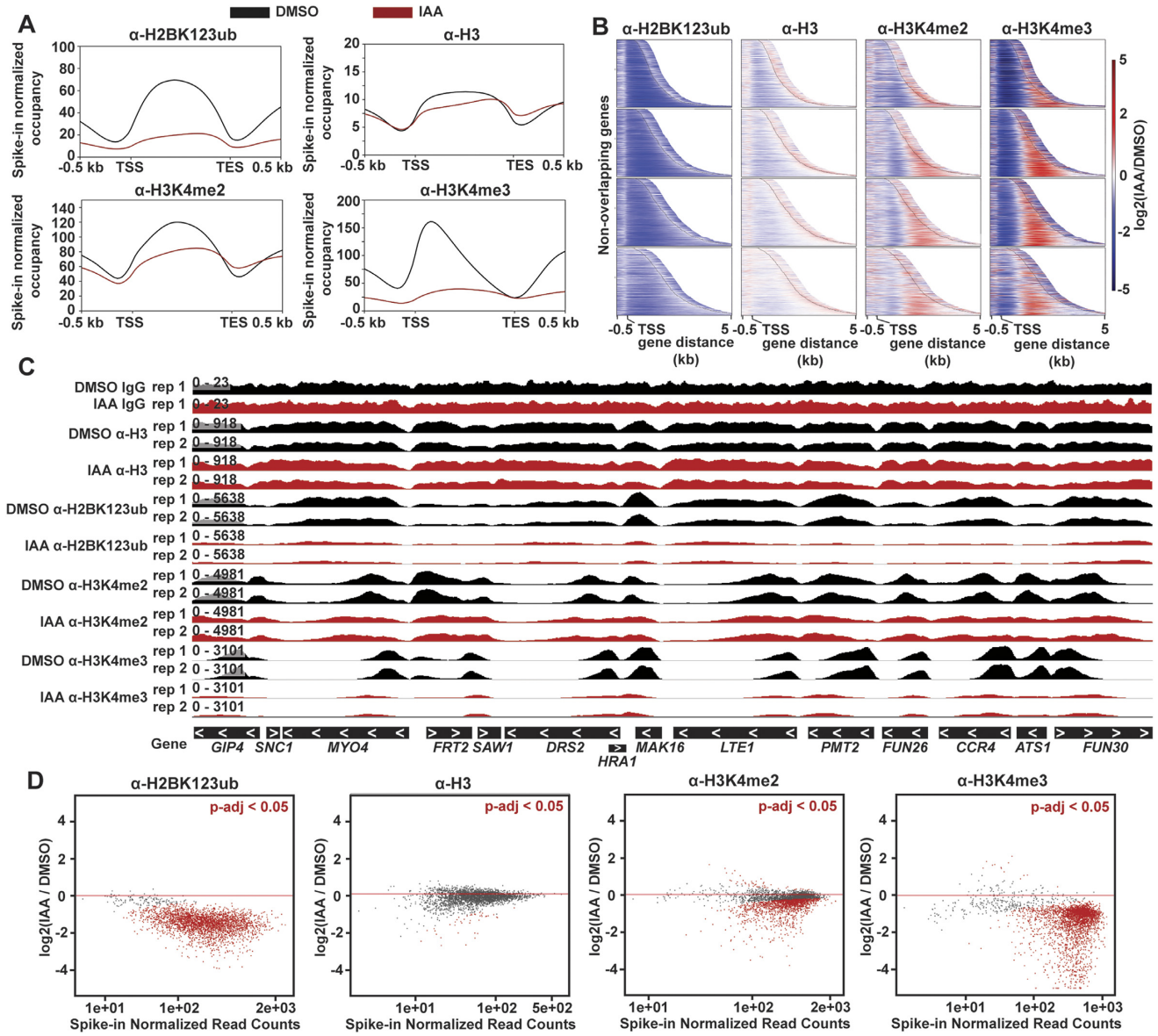

Figure 5. Acute depletion of Spt6 leads to changes in Paf1C-dependent histone modifications genome-wide. (**A**) Aggregation plots of spike-in normalized ChIP-seq data for H2BK123ub, total H3, H3K4me2, and H3K4me3. (**B**) Heatmaps of differential H2BK123ub, total H3, H3K4me2, and H3K4me3 occupancy (IAA vs DMSO). Genes are divided into quartiles based on Rpb1 occupancy (highest occupancy quartile on top) and sorted by length. Heatmaps show the region between the TSS and the cleavage and poly-adenylation site (labeled with a black line) +/- 500 bp and use a bin size of 25 bp. (**C**) Genome browser tracks of a region of chromosome 1 (chrI:84656–118640) showing spike-in normalized ChIP-seq occupancy for individual biological replicates. The IgG control data are the same as those shown in Figure 4E and are included here for completeness. (**D**) MA plots showing differential occupancy, determined by DESeq2 of spike-in normalized ChIP-seq data (IAA versus DMSO), for H2BK123ub, total H3, H3K4me2, and H3K4me3. Genes with statistically significant changes in occupancy (FDR adjusted P value ≤ 0.05) are colored red. (**A, B, D**) The results presented are derived from 3087 non-overlapping protein-coding genes (94) and were generated by averaging data from two biological replicates (strains KY4305 and KY4306).

different Paf1C subunits, Cdc73, Rtf1 and Ctr9, to CTD repeat peptides phosphorylated at positions Ser2 and Ser5 or Ser5 and Ser7 (33). The requirement for phosphorylation of serines 2, 5 and 7 for these *in vitro* interactions is consistent with the specificities of the kinases implicated by cell-based assays to be important for Paf1C recruitment. The peptide interacting region of Cdc73 mapped to amino acids 201–393, which overlap the structurally defined C-domain (amino acids 230–393) (42), and substitution of hydrophobic residues within the C-domain reduced Cdc73 occupancy at several active genes (33). While these studies support an interaction between Cdc73 and the phosphorylated CTD, interpretations are complicated by the ability of three different subunits to bind the same CTD peptides and the ability of these same subunits to bind to phosphorylated Spt5 peptides (33). Our BPA crosslinking data provide the first evidence for a direct interaction between the Cdc73 C-domain and Rpb1 *in vivo*. Using protease-cleavable forms of Rpb1, we mapped the interaction between Cdc73 R300 and Rpb1 to the linker region between the Rpb1 core and CTD. The

Rpb1 linker region is phosphorylated by Bur1 and interacts with the Spt6 tSH2 domain (82,98). From the Cdc73 side of the interaction, substitution of W321 to alanine greatly diminished the Cdc73-Rpb1 crosslink. Among a large number of amino acid substitutions tested in our previous mutational analysis of the C-domain, the Cdc73 W321A substitution was the only one to confer detectable sensitivity to the base analog 6-azauracil, a property shared by other elongation factor mutants (42). Compared to relevant single mutant strains, *cdc73-W321A rtf1Δ* double mutant strains exhibit enhanced sensitivity to 6-azauracil and lower levels of H3K36me3, consistent with the idea that Cdc73 and Rtf1 separably impact Paf1C recruitment and function (42). While our data support a direct and transcriptionally relevant interaction between Cdc73 R300 and the Rpb1 linker, they do not rule out contacts between other amino acids in Cdc73 and other domains in Rpb1, including the CTD.

Our search for Cdc73 interactors by *in vivo* BPA crosslinking also identified an interaction between Cdc73 and Spt6. Spt6 is an essential, conserved member of the Pol II elongation complex whose occupancy on chromatin correlates with that of Pol II (3–4,37–38). Spt6 promotes transcription elongation (17,90–91,99), interacts with histones and a co-regulatory protein Spn1 (100–103), stimulates Set2-mediated H3K36me3 (104–106), and functions as a histone chaperone to maintain chromatin integrity on active genes (89,107–108). To our knowledge, our results are the first demonstration of a direct interaction between Cdc73 and Spt6 *in vivo*. Importantly, a very recent cryo-EM analysis by Ehara *et al.* provided the first detailed structural insight into yeast Cdc73 within a Pol II elongation complex and revealed that the C-domain interacts with the Spt6 tSH2 domain near the point where the Rpb1 linker emerges (83). Consistent with this structure, we found that the crosslinking interaction we detected between Cdc73 and Spt6 *in vivo* was dependent on the Spt6 tSH2 domain. It is notable that the same BPA-substituted residue in Cdc73, R300, crosslinked to the Rpb1 linker and Spt6, and both crosslinks were greatly diminished by the W321A substitution and by absence of the Spt6 tSH2 domain. In the context of current structural information, our crosslinking results most likely reflect physical proximity among all three proteins in the form of a ternary interaction within the active elongation complex *in vivo* (4–5,83).

Using purified recombinant proteins, we demonstrated that an Spt6 derivative lacking the acidic, unstructured N-terminal region (66) can interact with Cdc73 *in vitro*. Through chemical crosslinking and structural modeling, we identified a putative interface between the Cdc73 C-domain and the YqgF, HhH and DLD domains of Spt6. Although an Spt6 derivative lacking these domains was completely defective for binding to Cdc73 *in vitro*, targeted mutational analysis of the predicted interface did not alter chromatin occupancy of Paf1C *in vivo* even in a sensitized background in which the Rtf1-Spt5 interaction has been mutationally compromised. The latter result might stem from redundancy in the molecular interface that allows minor perturbations to be tolerated. However, because the chemical crosslinking experiments did not detect contacts between Cdc73 and the Spt6 tSH2 domain, the biological importance of the interactions detected with the purified proteins remains unknown. Nonetheless, we cannot exclude a role for these interactions at an intermediate step in Pol II elongation complex assembly.

Our biochemical and crosslinking results led us to investigate a role for Spt6 in Paf1C recruitment and/or maintenance on chromatin. Previous studies showed that Paf1C occupancy on chromatin was diminished by the *S. cerevisiae spt6-1004* mutation, the analogous mutation in *Schizosaccharomyces pombe SPT6*, or depletion of Drosophila Spt6 by RNAi (47,92,99). These ChIP results are supported by a recent proteomic study, which showed a significant reduction in Pol II-associated Paf1C in strains containing the *spt6-1004* mutation, an in-frame deletion that removes the Spt6 HhH domain (109). While these studies indicate a role for Spt6, and possibly the HhH domain more directly, in controlling Paf1C occupancy on chromatin, interpretations are complicated by the instability of the Spt6-1004 protein and of some Paf1C subunits in *spt6-1004* mutant strains (47,109). We chose two alternative approaches to test the requirement for Spt6 in coupling Paf1C to Pol II. First, using the *spt6-50* mutation, we dissociated Spt6 from Pol II and observed a decrease in Paf1C occupancy on two active genes by ChIP-qPCR. Second, to rule out indirect effects caused by long-term absence of a functional Spt6 protein, we used the AID system to acutely deplete Spt6 and observed genome-wide loss of Paf1 occupancy. Unlike Paf1, Spt5 occupancy on chromatin was not decreased upon rapid Spt6 depletion, suggesting that Spt5 does not require Spt6 for its recruitment to Pol II. Under these conditions, effects on Paf1 occupancy cannot be easily explained by loss of the Rtf1-Spt5 interaction, although we cannot rule out conformational changes to the Rtf1–Spt5 interface in the absence of Spt6. Importantly, while our paper was under revision, a prominent role for Spt6 in controlling Paf1C occupancy on transcribed genes in human cancer cells was reported, strongly arguing that this is a conserved mechanism in the assembly of Pol II elongation complexes (110).

Consistent with findings by Jeronimo *et al.* (77), we found that loss of Spt6 broadly affects histone modification patterns genome-wide, including those that are Paf1C-dependent. Acute depletion of Spt6 caused a large reduction in H2BK123ub on gene bodies, which can be explained by the inability to reestablish this modification in the absence of Paf1C after pre-existing H2Bub marks are turned over by the deubiquitylases Ubp8 and Ubp10 (111). As noted previously (77), we also observed a redistribution of H3K4me2 and H3K4me3 toward the 3′ ends of genes in the absence of Spt6. The retention of H3K4me2 and H3K4me3, albeit in a mislocalized pattern, is consistent with the stable nature of these modifications in yeast (112). Therefore, through multiple activities, which include recruitment of Paf1C, recycling of histones during transcription elongation (77), and association with the histone chaperone Spn1 (94), Spt6 plays a major role in determining histone modification patterns genome-wide.

In conclusion, through the identification of interactions between Cdc73 and two components of the core Pol II elongation machinery, our findings provide new insights into the coupling of Paf1C to Pol II, a process that is important for the patterning of Paf1C-mediated histone modifications and the control of transcription elongation. Interest-

ingly, three mediators of Paf1C attachment to Pol II—the Spt5 CTR, the Rpb1 CTD, and the Rpb1 linker region, which binds to Spt6—are all targets of the Bur1/CDK9 kinase, providing an explanation for the strong requirement for this kinase in controlling the association of Paf1C with Pol II (31,33). Understanding why multiple interactions are required for incorporation of Paf1C into the elongation complex and how these interactions are regulated will be important areas for future study. Finally, we note that the Cdc73-Spt6 and Cdc73-Rpb1 interactions identified here offer Paf1C recruitment mechanisms independent of Rtf1, which might prove instrumental in human cells where hRtf1 is loosely associated with hPaf1C.

DATA AVAILABILITY

Strains and plasmids are available upon request. ChIP-seq data have been deposited in the Gene Expression Omnibus database under accession number GSE201436. The code used for the analysis of ChIP-seq data has been uploaded to the following Zenodo repository: https://doi.org/10.5281/zenodo.7675568. Information related to modeling of the Cdc73-Spt6 interaction, including PDB files, scripts, and crosslinking data, can be accessed at the following Zenodo repository: https://doi.org/10.5281/zenodo.7675568.

SUPPLEMENTARY DATA

Supplementary Data are available at NAR Online.

ACKNOWLEDGEMENTS

We thank Roni Lahr and Andrea Berman for advice on quantifying protein binding assays, Andrew VanDemark and members of his laboratory for sharing equipment and providing technical advice particularly on protein interaction assays, Craig Kaplan for the *RPB1*-TEV plasmid, Steve Buratowski for the *RPB1*-PreScission plasmid, Fred Winston and Nathan Clark for yeast strains, Tim Formosa, Grant Hartzog and John Woolford for antibodies, and Julia Seraly for assisting with the analysis of the *spt6* mutants. We are grateful for the helpful suggestions we have received from Frank Pugh, Olga Viktorovskaya, and Fred Winston. We also thank Craig Kaplan, Sarah Hainer, Miler Lee, members of their laboratories, and all members of the Arndt laboratory, especially Alex Francette, for many helpful discussions. This project used the University of Pittsburgh Health Sciences Sequencing Core at UPMC Children's Hospital of Pittsburgh for genomic sequencing experiments and was supported in part by the University of Pittsburgh Center for Research Computing through the resources provided.

FUNDING

National Institutes of Health [R01GM52593, R35GM141964 to K.M.A, F31GM129917 to M.A.E., R21CA261737, R35GM137905 to Y.S.]. Funding for open access charge: NIH [R35GM141964].
Conflict of interest statement. None declared.

REFERENCES

1. Chen,F.X., Smith,E.R. and Shilatifard,A. (2018) Born to run: control of transcription elongation by RNA polymerase II. *Nat. Rev. Mol. Cell Biol.*, **19**, 464–478.
2. Kujirai,T. and Kurumizaka,H. (2020) Transcription through the nucleosome. *Curr. Opin. Struct. Biol.*, **61**, 42–49.
3. Mayer,A., Lidschreiber,M., Siebert,M., Leike,K., Soding,J. and Cramer,P. (2010) Uniform transitions of the general RNA polymerase II transcription complex. *Nat. Struct. Mol. Biol.*, **17**, 1272–1278.
4. Vos,S.M., Farnung,L., Boehning,M., Wigge,C., Linden,A., Urlaub,H. and Cramer,P. (2018) Structure of activated transcription complex Pol II-DSIF-PAF-SPT6. *Nature*, **560**, 607–612.
5. Vos,S.M., Farnung,L., Linden,A., Urlaub,H. and Cramer,P. (2020) Structure of complete Pol II-DSIF-PAF-SPT6 transcription complex reveals RTF1 allosteric activation. *Nat. Struct. Mol. Biol.*, **27**, 668–677.
6. Costa,P.J. and Arndt,K.M. (2000) Synthetic lethal interactions suggest a role for the *Saccharomyces cerevisiae* Rtf1 protein in transcription elongation. *Genetics*, **156**, 535–547.
7. Krogan,N.J., Kim,M., Ahn,S.H., Zhong,G., Kobor,M.S., Cagney,G., Emili,A., Shilatifard,A., Buratowski,S. and Greenblatt,J.F. (2002) RNA polymerase II elongation factors of *Saccharomyces cerevisiae*: a targeted proteomics approach. *Mol. Cell. Biol.*, **22**, 6979–6992.
8. Mueller,C.L. and Jaehning,J.A. (2002) Ctr9, Rtf1, and Leo1 are components of the Paf1/RNA polymerase II complex. *Mol. Cell. Biol.*, **22**, 1971–1980.
9. Squazzo,S.L., Costa,P.J., Lindstrom,D.L., Kumer,K.E., Simic,R., Jennings,J.L., Link,A.J., Arndt,K.M. and Hartzog,G.A. (2002) The Paf1 complex physically and functionally associates with transcription elongation factors *in vivo*. *EMBO J.*, **21**, 1764–1774.
10. Francette,A.M., Tripplehorn,S.A. and Arndt,K.M. (2021) The Paf1 complex: a keystone of nuclear regulation operating at the interface of transcription and chromatin. *J. Mol. Biol.*, **433**, 166979.
11. Kim,J., Guermah,M. and Roeder,R.G. (2010) The human PAF1 complex acts in chromatin transcription elongation both independently and cooperatively with SII/TFIIS. *Cell*, **140**, 491–503.
12. Chen,F.X., Woodfin,A.R., Gardini,A., Rickels,R.A., Marshall,S.A., Smith,E.R., Shiekhattar,R. and Shilatifard,A. (2015) PAF1, a molecular regulator of promoter-proximal pausing by RNA polymerase II. *Cell*, **162**, 1003–1015.
13. Chen,F.X., Xie,P., Collings,C.K., Cao,K., Aoi,Y., Marshall,S.A., Rendleman,E.J., Ugarenko,M., Ozark,P.A., Zhang,A. *et al.* (2017) PAF1 regulation of promoter-proximal pause release via enhancer activation. *Science*, **357**, 1294–1298.
14. Hou,L., Wang,Y., Liu,Y., Zhang,N., Shamovsky,I., Nudler,E., Tian,B. and Dynlacht,B.D. (2019) Paf1C regulates RNA polymerase II progression by modulating elongation rate. *Proc. Natl. Acad. Sci. U.S.A.*, **116**, 14583–14592.
15. Wang,Z., Song,A., Xu,H., Hu,S., Tao,B., Peng,L., Wang,J., Li,J., Yu,J., Wang,L. *et al.* (2022) Coordinated regulation of RNA polymerase II pausing and elongation progression by PAF1. *Sci. Adv.*, **8**, eabm5504.
16. Yu,M., Yang,W., Ni,T., Tang,Z., Nakadai,T., Zhu,J. and Roeder,R.G. (2015) RNA polymerase II-associated factor 1 regulates the release and phosphorylation of paused RNA polymerase II. *Science*, **350**, 1383–1386.
17. Zumer,K., Maier,K.C., Farnung,L., Jaeger,M.G., Rus,P., Winter,G. and Cramer,P. (2021) Two distinct mechanisms of RNA polymerase II elongation stimulation *in vivo*. *Mol. Cell*, **81**, 3096–3109.
18. Endres,T., Solvie,D., Heidelberger,J.B., Andrioletti,V., Baluapuri,A., Ade,C.P., Muhar,M., Eilers,U., Vos,S.M., Cramer,P. *et al.* (2021) Ubiquitylation of MYC couples transcription elongation with double-strand break repair at active promoters. *Mol. Cell*, **81**, 830–844.
19. Fischl,H., Howe,F.S., Furger,A. and Mellor,J. (2017) Paf1 has distinct roles in transcription elongation and differential transcript fate. *Mol. Cell*, **65**, 685–698.
20. Penheiter,K.L., Washburn,T.M., Porter,S.E., Hoffman,M.G. and Jaehning,J.A. (2005) A posttranscriptional role for the yeast Paf1-RNA polymerase II complex is revealed by identification of primary targets. *Mol. Cell*, **20**, 213–223.

21. Sheldon,K.E., Mauger,D.M. and Arndt,K.M. (2005) A requirement for the *Saccharomyces cerevisiae* Paf1 complex in snoRNA 3′ end formation. *Mol. Cell*, **20**, 225–236.
22. van den Heuvel,D., Spruijt,C.G., Gonzalez-Prieto,R., Kragten,A., Paulsen,M.T., Zhou,D., Wu,H., Apelt,K., van der Weegen,Y., Yang,K. *et al.* (2021) A CSB-PAF1C axis restores processive transcription elongation after DNA damage repair. *Nat. Commun.*, **12**, 1342.
23. Yang,Y., Li,W., Hoque,M., Hou,L., Shen,S., Tian,B. and Dynlacht,B.D. (2016) PAF complex plays novel subunit-specific roles in alternative cleavage and polyadenylation. *PLoS Genet.*, **12**, e1005794.
24. Chu,Y., Simic,R., Warner,M.H., Arndt,K.M. and Prelich,G. (2007) Regulation of histone modification and cryptic transcription by the Bur1 and Paf1 complexes. *EMBO J.*, **26**, 4646–4656.
25. Smolle,M. and Workman,J.L. (2013) Transcription-associated histone modifications and cryptic transcription. *Biochim. Biophys. Acta*, **1829**, 84–97.
26. Piro,A.S., Mayekar,M.K., Warner,M.H., Davis,C.P. and Arndt,K.M. (2012) Small region of Rtf1 protein can substitute for complete Paf1 complex in facilitating global histone H2B ubiquitylation in yeast. *Proc. Natl. Acad. Sci. U.S.A.*, **109**, 10837–10842.
27. Van Oss,S.B., Shirra,M.K., Bataille,A.R., Wier,A.D., Yen,K., Vinayachandran,V., Byeon,I.L., Cucinotta,C.E., Heroux,A., Jeon,J. *et al.* (2016) The histone modification domain of Paf1 complex subunit Rtf1 directly stimulates H2B ubiquitylation through an interaction with Rad6. *Mol. Cell*, **64**, 815–825.
28. Warner,M.H., Roinick,K.L. and Arndt,K.M. (2007) Rtf1 is a multifunctional component of the Paf1 complex that regulates gene expression by directing cotranscriptional histone modification. *Mol. Cell. Biol.*, **27**, 6103–6115.
29. Chen,F., Liu,B., Guo,L., Ge,X., Feng,W., Li,D.F., Zhou,H. and Long,J. (2021) Biochemical insights into Paf1 complex-induced stimulation of Rad6/Bre1-mediated H2B monoubiquitination. *Proc. Natl. Acad. Sci. U.S.A.*, **118**, e2025291118.
30. Worden,E.J. and Wolberger,C. (2019) Activation and regulation of H2B-ubiquitin-dependent histone methyltransferases. *Curr. Opin. Struct. Biol.*, **59**, 98–106.
31. Laribee,R.N., Krogan,N.J., Xiao,T., Shibata,Y., Hughes,T.R., Greenblatt,J.F. and Strahl,B.D. (2005) BUR kinase selectively regulates H3 K4 trimethylation and H2B ubiquitylation through recruitment of the PAF elongation complex. *Curr. Biol.*, **15**, 1487–1493.
32. Liu,Y., Warfield,L., Zhang,C., Luo,J., Allen,J., Lang,W.H., Ranish,J., Shokat,K.M. and Hahn,S. (2009) Phosphorylation of the transcription elongation factor Spt5 by yeast Bur1 kinase stimulates recruitment of the PAF complex. *Mol. Cell. Biol.*, **29**, 4852–4863.
33. Qiu,H., Hu,C., Gaur,N.A. and Hinnebusch,A.G. (2012) Pol II CTD kinases Bur1 and Kin28 promote Spt5 CTR-independent recruitment of Paf1 complex. *EMBO J.*, **31**, 3494–3505.
34. Tellier,M., Zaborowska,J., Caizzi,L., Mohammad,E., Velychko,T., Schwalb,B., Ferrer-Vicens,I., Blears,D., Nojima,T., Cramer,P. *et al.* (2020) CDK12 globally stimulates RNA polymerase II transcription elongation and carboxyl-terminal domain phosphorylation. *Nucleic Acids Res.*, **48**, 7712–7727.
35. Zhou,K., Kuo,W.H., Fillingham,J. and Greenblatt,J.F. (2009) Control of transcriptional elongation and cotranscriptional histone modification by the yeast BUR kinase substrate Spt5. *Proc. Natl. Acad. Sci. U.S.A.*, **106**, 6956–6961.
36. Decker,T.M. (2021) Mechanisms of transcription elongation factor DSIF (Spt4-Spt5). *J. Mol. Biol.*, **433**, 166657.
37. Duina,A.A. (2011) Histone chaperones Spt6 and FACT: similarities and differences in modes of action at transcribed genes. *Genet. Res. Int.*, **2011**, 625210.
38. Hammond,C.M., Stromme,C.B., Huang,H., Patel,D.J. and Groth,A. (2017) Histone chaperone networks shaping chromatin function. *Nat. Rev. Mol. Cell Biol.*, **18**, 141–158.
39. Mayekar,M.K., Gardner,R.G. and Arndt,K.M. (2013) The recruitment of the *Saccharomyces cerevisiae* Paf1 complex to active genes requires a domain of Rtf1 that directly interacts with the Spt4-Spt5 complex. *Mol. Cell. Biol.*, **33**, 3259–3273.
40. Wier,A.D., Mayekar,M.K., Heroux,A., Arndt,K.M. and VanDemark,A.P. (2013) Structural basis for Spt5-mediated recruitment of the Paf1 complex to chromatin. *Proc. Natl. Acad. Sci. U.S.A.*, **110**, 17290–17295.
41. Cao,Q.F., Yamamoto,J., Isobe,T., Tateno,S., Murase,Y., Chen,Y., Handa,H. and Yamaguchi,Y. (2015) Characterization of the human transcription elongation factor Rtf1: evidence for nonoverlapping functions of Rtf1 and the Paf1 complex. *Mol. Cell. Biol.*, **35**, 3459–3470.
42. Amrich,C.G., Davis,C.P., Rogal,W.P., Shirra,M.K., Heroux,A., Gardner,R.G., Arndt,K.M. and VanDemark,A.P. (2012) Cdc73 subunit of Paf1 complex contains C-terminal Ras-like domain that promotes association of Paf1 complex with chromatin. *J. Biol. Chem.*, **287**, 10863–10875.
43. Winston,F., Dollard,C. and Ricupero-Hovasse,S.L. (1995) Construction of a set of convenient *Saccharomyces cerevisiae* strains that are isogenic to S288C. *Yeast*, **11**, 53–55.
44. Lundblad,V., Hartzog,G. and Moqtaderi,Z. (2001) Manipulation of cloned yeast DNA. *Curr. Protoc. Mol. Biol.*, **Chapter 13**, Unit13.10.
45. Rose,M.D., Winston,F. and Hieter,P. (1990) In: *Methods in Yeast Genetics: A Laboratory Course Manual*. Cold Spring Harbor Laboratory Press, NY.
46. Storici,F. and Resnick,M.A. (2006) The *delitto perfetto* approach to *in vivo* site-directed mutagenesis and chromosome rearrangements with synthetic oligonucleotides in yeast. *Methods Enzymol.*, **409**, 329–345.
47. Kaplan,C.D., Holland,M.J. and Winston,F. (2005) Interaction between transcription elongation factors and mRNA 3′-end formation at the *Saccharomyces cerevisiae GAL10-GAL7* locus. *J. Biol. Chem.*, **280**, 913–922.
48. Sikorski,R.S. and Boeke,J.D. (1991) *In vitro* mutagenesis and plasmid shuffling: from cloned gene to mutant yeast. *Methods Enzymol.*, **194**, 302–318.
49. Sikorski,R.S. and Hieter,P. (1989) A system of shuttle vectors and yeast host strains designed for efficient manipulation of DNA in *Saccharomyces cerevisiae*. *Genetics*, **122**, 19–27.
50. Cox,J.S., Chapman,R.E. and Walter,P. (1997) The unfolded protein response coordinates the production of endoplasmic reticulum protein and endoplasmic reticulum membrane. *Mol. Biol. Cell*, **8**, 1805–1814.
51. Kushnirov,V.V. (2000) Rapid and reliable protein extraction from yeast. *Yeast*, **16**, 857–860.
52. Cucinotta,C.E., Hildreth,A.E., McShane,B.M., Shirra,M.K. and Arndt,K.M. (2019) The nucleosome acidic patch directly interacts with subunits of the Paf1 and FACT complexes and controls chromatin architecture *in vivo*. *Nucleic Acids Res.*, **47**, 8410–8423.
53. Chin,J.W., Cropp,T.A., Anderson,J.C., Mukherji,M., Zhang,Z. and Schultz,P.G. (2003) An expanded eukaryotic genetic code. *Science*, **301**, 964–967.
54. Fernandez-Martinez,J., Kim,S.J., Shi,Y., Upla,P., Pellarin,R., Gagnon,M., Chemmama,I.E., Wang,J., Nudelman,I., Zhang,W. *et al.* (2016) Structure and function of the nuclear pore complex cytoplasmic mRNA export platform. *Cell*, **167**, 1215–1228.
55. Shi,Y., Fernandez-Martinez,J., Tjioe,E., Pellarin,R., Kim,S.J., Williams,R., Schneidman-Duhovny,D., Sali,A., Rout,M.P. and Chait,B.T. (2014) Structural characterization by cross-linking reveals the detailed architecture of a coatomer-related heptameric module from the nuclear pore complex. *Mol. Cell. Proteomics*, **13**, 2927–2943.
56. Shi,Y., Pellarin,R., Fridy,P.C., Fernandez-Martinez,J., Thompson,M.K., Li,Y., Wang,Q.J., Sali,A., Rout,M.P. and Chait,B.T. (2015) A strategy for dissecting the architectures of native macromolecular assemblies. *Nat. Methods*, **12**, 1135–1138.
57. Xiang,Y., Nambulli,S., Xiao,Z., Liu,H., Sang,Z., Duprex,W.P., Schneidman-Duhovny,D., Zhang,C. and Shi,Y. (2020) Versatile and multivalent nanobodies efficiently neutralize SARS-CoV-2. *Science*, **370**, 1479–1484.
58. Xiang,Y., Sang,Z., Bitton,L., Xu,J., Liu,Y., Schneidman-Duhovny,D. and Shi,Y. (2021) Integrative proteomics identifies thousands of distinct, multi-epitope, and high-affinity nanobodies. *Cell Syst.*, **12**, 220–234.
59. Chen,Z.L., Meng,J.M., Cao,Y., Yin,J.L., Fang,R.Q., Fan,S.B., Liu,C., Zeng,W.F., Ding,Y.H., Tan,D. *et al.* (2019) A high-speed search engine pLink 2 with systematic evaluation for proteome-scale identification of cross-linked peptides. *Nat. Commun.*, **10**, 3404.

60. Russel,D., Lasker,K., Webb,B., Velazquez-Muriel,J., Tjioe,E., Schneidman-Duhovny,D., Peterson,B. and Sali,A. (2012) Putting the pieces together: integrative modeling platform software for structure determination of macromolecular assemblies. *PLoS Biol.*, **10**, e1001244.
61. Roy,A., Kucukural,A. and Zhang,Y. (2010) I-TASSER: a unified platform for automated protein structure and function prediction. *Nat. Protoc.*, **5**, 725–738.
62. Yang,J., Yan,R., Roy,A., Xu,D., Poisson,J. and Zhang,Y. (2015) The I-TASSER Suite: protein structure and function prediction. *Nat. Methods*, **12**, 7–8.
63. Zhang,Y. (2008) I-TASSER server for protein 3D structure prediction. *BMC Bioinf.*, **9**, 40.
64. Deng,P., Zhou,Y., Jiang,J., Li,H., Tian,W., Cao,Y., Qin,Y., Kim,J., Roeder,R.G., Patel,D.J. *et al.* (2018) Transcriptional elongation factor Paf1 core complex adopts a spirally wrapped solenoidal topology. *Proc. Natl. Acad. Sci. U.S.A.*, **115**, 9998–10003.
65. Sun,W., Kuang,X.L., Liu,Y.P., Tian,L.F., Yan,X.X. and Xu,W. (2017) Crystal structure of the N-terminal domain of human CDC73 and its implications for the hyperparathyroidism-jaw tumor (HPT-JT) syndrome. *Sci. Rep.*, **7**, 15638.
66. Close,D., Johnson,S.J., Sdano,M.A., McDonald,S.M., Robinson,H., Formosa,T. and Hill,C.P. (2011) Crystal structures of the *S.cerevisiae* Spt6 core and C-terminal tandem SH2 domain. *J. Mol. Biol.*, **408**, 697–713.
67. Li,Z., Ye,Y. and Godzik,A. (2006) Flexible structural neighborhood–a database of protein structural similarities and alignments. *Nucleic Acids Res.*, **34**, D277–D280.
68. Ye,Y. and Godzik,A. (2003) Flexible structure alignment by chaining aligned fragment pairs allowing twists. *Bioinformatics*, **19**, ii246–i255.
69. Ye,Y. and Godzik,A. (2004) Database searching by flexible protein structure alignment. *Protein Sci.*, **13**, 1841–1850.
70. Ye,Y. and Godzik,A. (2004) FATCAT: a web server for flexible structure comparison and structure similarity searching. *Nucleic Acids Res.*, **32**, W582–W585.
71. Shirra,M.K., Kocik,R.A., Ellison,M.A. and Arndt,K.M. (2021) Opposing functions of the Hda1 complex and histone H2B mono-ubiquitylation in regulating cryptic transcription in *Saccharomyces cerevisiae*. *G3 (Bethesda)*, **11**, jkab298.
72. Shirra,M.K., Rogers,S.E., Alexander,D.E. and Arndt,K.M. (2005) The Snf1 protein kinase and Sit4 protein phosphatase have opposing functions in regulating TATA-binding protein association with the *Saccharomyces cerevisiae INO1* promoter. *Genetics*, **169**, 1957–1972.
73. Komarnitsky,P., Cho,E.J. and Buratowski,S. (2000) Different phosphorylated forms of RNA polymerase II and associated mRNA processing factors during transcription. *Genes Dev.*, **14**, 2452–2460.
74. Cucinotta,C.E., Young,A.N., Klucevsek,K.M. and Arndt,K.M. (2015) The nucleosome acidic patch regulates the H2B K123 monoubiquitylation cascade and transcription elongation in *Saccharomyces cerevisiae*. *PLoS Genet.*, **11**, e1005420.
75. Langmead,B. and Salzberg,S.L. (2012) Fast gapped-read alignment with Bowtie 2. *Nat. Methods*, **9**, 357–359.
76. 1000 Genome Project Data Processing Subgroup, Li,H., Handsaker,B., Wysoker,A., Fennell,T., Ruan,J., Homer,N., Marth,G., Abecasis,G. and Durbin,R.(2009) The sequence alignment/map format and samtools. *Bioinformatics*, **25**, 2078–2079.
77. Jeronimo,C., Poitras,C. and Robert,F. (2019) Histone recycling by FACT and Spt6 during transcription prevents the scrambling of histone modifications. *Cell Rep.*, **28**, 1206–1218.
78. Ramirez,F., Dundar,F., Diehl,S., Gruning,B.A. and Manke,T. (2014) deepTools: a flexible platform for exploring deep-sequencing data. *Nucleic Acids Res.*, **42**, W187–W191.
79. Ramirez,F., Ryan,D.P., Gruning,B., Bhardwaj,V., Kilpert,F., Richter,A.S., Heyne,S., Dundar,F. and Manke,T. (2016) deepTools2: a next generation web server for deep-sequencing data analysis. *Nucleic Acids Res.*, **44**, W160–W165.
80. Thorvaldsdottir,H., Robinson,J.T. and Mesirov,J.P. (2013) Integrative Genomics Viewer (IGV): high-performance genomics data visualization and exploration. *Brief. Bioinform*, **14**, 178–192.
81. Suh,H., Ficarro,S.B., Kang,U.B., Chun,Y., Marto,J.A. and Buratowski,S. (2016) Direct analysis of phosphorylation sites on the Rpb1 C-terminal domain of RNA polymerase II. *Mol. Cell*, **61**, 297–304.
82. Sdano,M.A., Fulcher,J.M., Palani,S., Chandrasekharan,M.B., Parnell,T.J., Whitby,F.G., Formosa,T. and Hill,C.P. (2017) A novel SH2 recognition mechanism recruits Spt6 to the doubly phosphorylated RNA polymerase II linker at sites of transcription. *eLife*, **6**, e28723.
83. Ehara,H., Kujirai,T., Shirouzu,M., Kurumizaka,H. and Sekine,S.I. (2022) Structural basis of nucleosome disassembly and reassembly by RNAPII elongation complex with FACT. *Science*, **377**, eabp9466.
84. Dengl,S., Mayer,A., Sun,M. and Cramer,P. (2009) Structure and *in vivo* requirement of the yeast Spt6 SH2 domain. *J. Mol. Biol.*, **389**, 211–225.
85. Diebold,M.L., Loeliger,E., Koch,M., Winston,F., Cavarelli,J. and Romier,C. (2010) Noncanonical tandem SH2 enables interaction of elongation factor Spt6 with RNA polymerase II. *J. Biol. Chem.*, **285**, 38389–38398.
86. Liu,J., Zhang,J., Gong,Q., Xiong,P., Huang,H., Wu,B., Lu,G., Wu,J. and Shi,Y. (2011) Solution structure of tandem SH2 domains from Spt6 protein and their binding to the phosphorylated RNA polymerase II C-terminal domain. *J. Biol. Chem.*, **286**, 29218–29226.
87. Sun,M., Lariviere,L., Dengl,S., Mayer,A. and Cramer,P. (2010) A tandem SH2 domain in transcription elongation factor Spt6 binds the phosphorylated RNA polymerase II C-terminal repeat domain (CTD). *J. Biol. Chem.*, **285**, 41597–41603.
88. Nishimura,K., Fukagawa,T., Takisawa,H., Kakimoto,T. and Kanemaki,M. (2009) An auxin-based degron system for the rapid depletion of proteins in nonplant cells. *Nat. Methods*, **6**, 917–922.
89. Doris,S.M., Chuang,J., Viktorovskaya,O., Murawska,M., Spatt,D., Churchman,L.S. and Winston,F. (2018) Spt6 is required for the fidelity of promoter selection. *Mol. Cell*, **72**, 687–699.
90. Endoh,M., Zhu,W., Hasegawa,J., Watanabe,H., Kim,D.K., Aida,M., Inukai,N., Narita,T., Yamada,T., Furuya,A. *et al.* (2004) Human Spt6 stimulates transcription elongation by RNA polymerase II *in vitro*. *Mol. Cell. Biol.*, **24**, 3324–3336.
91. Narain,A., Bhandare,P., Adhikari,B., Backes,S., Eilers,M., Dolken,L., Schlosser,A., Erhard,F., Baluapuri,A. and Wolf,E. (2021) Targeted protein degradation reveals a direct role of SPT6 in RNAPII elongation and termination. *Mol. Cell*, **81**, 3110–3127.
92. DeGennaro,C.M., Alver,B.H., Marguerat,S., Stepanova,E., Davis,C.P., Bahler,J., Park,P.J. and Winston,F. (2013) Spt6 regulates intragenic and antisense transcription, nucleosome positioning, and histone modifications genome-wide in fission yeast. *Mol. Cell. Biol.*, **33**, 4779–4792.
93. Kato,H., Okazaki,K., Iida,T., Nakayama,J., Murakami,Y. and Urano,T. (2013) Spt6 prevents transcription-coupled loss of posttranslationally modified histone H3. *Sci. Rep.*, **3**, 2186.
94. Reim,N.I., Chuang,J., Jain,D., Alver,B.H., Park,P.J. and Winston,F. (2020) The conserved elongation factor Spn1 is required for normal transcription, histone modifications, and splicing in *Saccharomyces cerevisiae*. *Nucleic Acids Res.*, **48**, 10241–10258.
95. Mueller,C.L., Porter,S.E., Hoffman,M.G. and Jaehning,J.A. (2004) The Paf1 complex has functions independent of actively transcribing RNA polymerase II. *Mol. Cell*, **14**, 447–456.
96. Joo,Y.J., Ficarro,S.B., Chun,Y., Marto,J.A. and Buratowski,S. (2019) *In vitro* analysis of RNA polymerase II elongation complex dynamics. *Genes Dev.*, **33**, 578–589.
97. Harlen,K.M. and Churchman,L.S. (2017) The code and beyond: transcription regulation by the RNA polymerase II carboxy-terminal domain. *Nat. Rev. Mol. Cell Biol.*, **18**, 263–273.
98. Chun,Y., Joo,Y.J., Suh,H., Batot,G., Hill,C.P., Formosa,T. and Buratowski,S. (2019) Selective kinase inhibition shows that Bur1 (Cdk9) phosphorylates the Rpb1 linker *in vivo*. *Mol. Cell. Biol.*, **39**, e00602-18.
99. Ardehali,M.B., Yao,J., Adelman,K., Fuda,N.J., Petesch,S.J., Webb,W.W. and Lis,J.T. (2009) Spt6 enhances the elongation rate of RNA polymerase II *in vivo*. *EMBO J.*, **28**, 1067–1077.
100. Bortvin,A. and Winston,F. (1996) Evidence that Spt6p controls chromatin structure by a direct interaction with histones. *Science*, **272**, 1473–1476.
101. Diebold,M.L., Koch,M., Loeliger,E., Cura,V., Winston,F., Cavarelli,J. and Romier,C. (2010) The structure of an Iws1/Spt6 complex reveals an interaction domain conserved in TFIIS, Elongin A and Med26. *EMBO J.*, **29**, 3979–3991.
102. McCullough,L., Connell,Z., Petersen,C. and Formosa,T. (2015) The abundant histone chaperones Spt6 and FACT collaborate to

assemble, inspect, and maintain chromatin structure in *Saccharomyces cerevisiae*. *Genetics*, **201**, 1031–1045.
103. McDonald,S.M., Close,D., Xin,H., Formosa,T. and Hill,C.P. (2010) Structure and biological importance of the Spn1-Spt6 interaction, and its regulatory role in nucleosome binding. *Mol. Cell*, **40**, 725–735.
104. Chu,Y., Sutton,A., Sternglanz,R. and Prelich,G. (2006) The BUR1 cyclin-dependent protein kinase is required for the normal pattern of histone methylation by SET2. *Mol. Cell. Biol.*, **26**, 3029–3038.
105. Gopalakrishnan,R., Marr,S.K., Kingston,R.E. and Winston,F. (2019) A conserved genetic interaction between Spt6 and Set2 regulates H3K36 methylation. *Nucleic Acids Res.*, **47**, 3888–3903.
106. Youdell,M.L., Kizer,K.O., Kisseleva-Romanova,E., Fuchs,S.M., Duro,E., Strahl,B.D. and Mellor,J. (2008) Roles for Ctk1 and Spt6 in regulating the different methylation states of histone H3 lysine 36. *Mol. Cell. Biol.*, **28**, 4915–4926.
107. Kaplan,C.D., Laprade,L. and Winston,F. (2003) Transcription elongation factors repress transcription initiation from cryptic sites. *Science*, **301**, 1096–1099.
108. Viktorovskaya,O., Chuang,J., Jain,D., Reim,N.I., Lopez-Rivera,F., Murawska,M., Spatt,D., Churchman,L.S., Park,P.J. and Winston,F. (2021) Essential histone chaperones collaborate to regulate transcription and chromatin integrity. *Genes Dev.*, **35**, 698–712.
109. Gopalakrishnan,R. and Winston,F. (2021) The histone chaperone Spt6 is required for normal recruitment of the capping enzyme Abd1 to transcribed regions. *J. Biol. Chem.*, **297**, 101205.
110. Aoi,Y., Shah,A.P., Ganesan,S., Soliman,S.H.A., Cho,B.K., Goo,Y.A., Kelleher,N.L. and Shilatifard,A. (2022) SPT6 functions in transcriptional pause/release via PAF1C recruitment. *Mol. Cell*, **82**, 3412–3423.
111. Schulze,J.M., Hentrich,T., Nakanishi,S., Gupta,A., Emberly,E., Shilatifard,A. and Kobor,M.S. (2011) Splitting the task: Ubp8 and Ubp10 deubiquitinate different cellular pools of H2BK123. *Genes Dev.*, **25**, 2242–2247.
112. Ng,H.H., Robert,F., Young,R.A. and Struhl,K. (2003) Targeted recruitment of Set1 histone methylase by elongating Pol II provides a localized mark and memory of recent transcriptional activity. *Mol. Cell*, **11**, 709–719.